

# Tissue damage negatively regulates LPS-induced macrophage necroptosis

Z Li<sup>1,2,3</sup>, MJ Scott<sup>1</sup>, EK Fan<sup>4</sup>, Y Li<sup>1,2</sup>, J Liu<sup>3</sup>, G Xiao<sup>5,6</sup>, S Li<sup>7</sup>, TR Billiar<sup>1,8</sup>, MA Wilson<sup>1,2</sup>, Y Jiang<sup>\*,3</sup> and J Fan<sup>\*,1,2,8</sup>

Infection is a common clinical complication following tissue damage resulting from surgery and severe trauma. Studies have suggested that cell pre-activation by antecedent trauma/tissue damage profoundly impacts the response of innate immune cells to a secondary infectious stimulus. Cell necroptosis, a form of regulated inflammatory cell death, is one of the mechanisms that control cell release of inflammatory mediators from important innate immune executive cells such as macrophages (M $\phi$ ), which critically regulate the progress of inflammation. In this study, we investigated the mechanism and role of trauma/tissue damage in the regulation of LPS-induced M $\phi$  necroptosis using a mouse model simulating long-bone fracture. We demonstrate that LPS acting through Toll-like receptor (TLR) 4 promotes M $\phi$  necroptosis. However, necroptosis is ameliorated by high-mobility group box 1 (HMGB1) release from damaged tissue. We show that HMGB1 acting through cell surface receptor for advanced glycation end products (RAGE) upregulates caveolin-1 expression, which in turn induces caveolae-mediated TLR4 internalization and desensitization to decrease M $\phi$  necroptosis. We further show that RAGE-MyD88 activation of Cdc42 and subsequent activation of transcription factor Sp1 serves as a mechanism underlying caveolin-1 transcriptional upregulation. These results reveal a previous unidentified protective role of damage-associated molecular pattern (DAMP) molecules in restricting inflammation in response to exogenous pathogen-associated molecular pattern molecules.

*Cell Death and Differentiation* (2016) 23, 1428–1447; doi:10.1038/cdd.2016.21; published online 4 March 2016

Infection is a common complication following tissue damage resulting from surgery and severe trauma.<sup>1</sup> Infection triggers the innate immune system to release large amounts of pro-inflammatory mediators that can have deadly consequences, including systemic inflammatory response syndrome and organ failure. Studies have suggested that cell pre-activation caused by antecedent trauma/tissue damage profoundly impacts the response of the innate immune cells to a secondary infectious stimulus, often in a form of enhanced inflammation.<sup>2</sup> Macrophages (M $\phi$ ), important innate immune executive cells, release pro-inflammatory mediators including cytokines and endogenous danger molecules, and critically regulate the progress of inflammation. Cell necroptosis, a form of regulated inflammatory cell death, is one mechanism that controls cell release of inflammatory mediators.<sup>3</sup> M $\phi$  necroptosis features RIPK1 activation and necrosome formation, followed by a loss of plasma membrane integrity and the release of cell contents into the extracellular space, which causes increased inflammation.<sup>4</sup> It has been reported that lipopolysaccharide (LPS) acting through Toll-like receptor (TLR) 4 signaling induces M $\phi$  necroptosis.<sup>5</sup> However, the

effect of antecedent trauma on the LPS-induced M $\phi$  necroptosis has yet to be addressed.

High mobility group box 1 (HMGB1), a highly conserved ubiquitous protein present in the nucleus and cytoplasm of nearly all cell types, is the prototypic damage-associated molecular pattern (DAMP)<sup>6</sup> released by damaged tissues.<sup>7</sup> During tissue injury, HMGB1 is released from cells and serves as a necessary and sufficient mediator of inflammation to induce a variety of cellular responses including cell chemotaxis and the release of pro-inflammatory cytokines.<sup>8,9</sup> Inflammatory functions of HMGB1 are mediated by binding to cell surface receptors, including the receptor for advanced glycation end products (RAGE), Toll-like receptor (TLR)2, TLR4, and TLR9.

RAGE is a type I transmembrane protein and a member of the immunoglobulin superfamily expressed in many cell populations including endothelial cells, vascular smooth muscle cells, neurons, neutrophils, and macrophages/monocytes.<sup>10</sup> RAGE has been implicated as a receptor mediating the chemotaxis and cytokine activity of HMGB1 in both M $\phi$  and tumor cells.<sup>11</sup> RAGE engagement by multiple

<sup>1</sup>Department of Surgery, University of Pittsburgh School of Medicine, Pittsburgh, PA 15213, USA; <sup>2</sup>Research and Development, Veterans Affairs Pittsburgh Healthcare System, Pittsburgh, PA 15240, USA; <sup>3</sup>Department of Pathophysiology, Southern Medical University, Guangzhou 510515, China; <sup>4</sup>University of Pittsburgh School of Arts and Science, Pittsburgh, PA 15213, USA; <sup>5</sup>Department of Biology and Shenzhen Key Laboratory of Cell Microenvironment, South University of Science and Technology of China, Shenzhen 518055, China; <sup>6</sup>Department of Biochemistry, Rush University Medical Center, Chicago, IL 60612, USA; <sup>7</sup>Center for Pharmacogenetics, Department of Pharmaceutical Sciences, University of Pittsburgh School of Pharmacy, Pittsburgh, PA 15261, USA and <sup>8</sup>McGowan Institute for Regenerative Medicine, University of Pittsburgh, Pittsburgh, PA 15219, USA

\*Corresponding author: Y Jiang or J Fan, Department of Surgery, University of Pittsburgh School of Medicine, Building 1, 2W109 (151U-L), University Drive, VAPHS, Pittsburgh 15240, USA. E-mail: jiang48231@163.com or jif7@pitt.edu

**Abbreviations:** BCM, bone-crush mixture; BMDM, bone marrow-derived macrophage; Cdc42, cell division control protein 42 homolog; DAMPs, damage-associated molecular patterns; HMGB1, high-mobility group box 1; LPS, lipopolysaccharides; M $\phi$ , macrophages; MLKL, mixed lineage kinase domain-like protein; MyD88, myeloid differentiation primary response gene 88; PAMPs, pathogen-associated molecular patterns; PF, pseudo-fracture; PM $\phi$ , peritoneal macrophages; RAGE, receptor for advanced glycation end product; RIPK1, receptor-interacting serine/threonine-protein kinase 1; RIPK3, receptor-interacting serine/threonine-protein kinase 3; SIRS, systemic inflammatory response syndrome; Sp1, specificity protein 1; TLR4, Toll-like receptor 4

Received 28.8.15; revised 24.1.16; accepted 02.2.16; Edited by J Silke; published online 04.3.2016

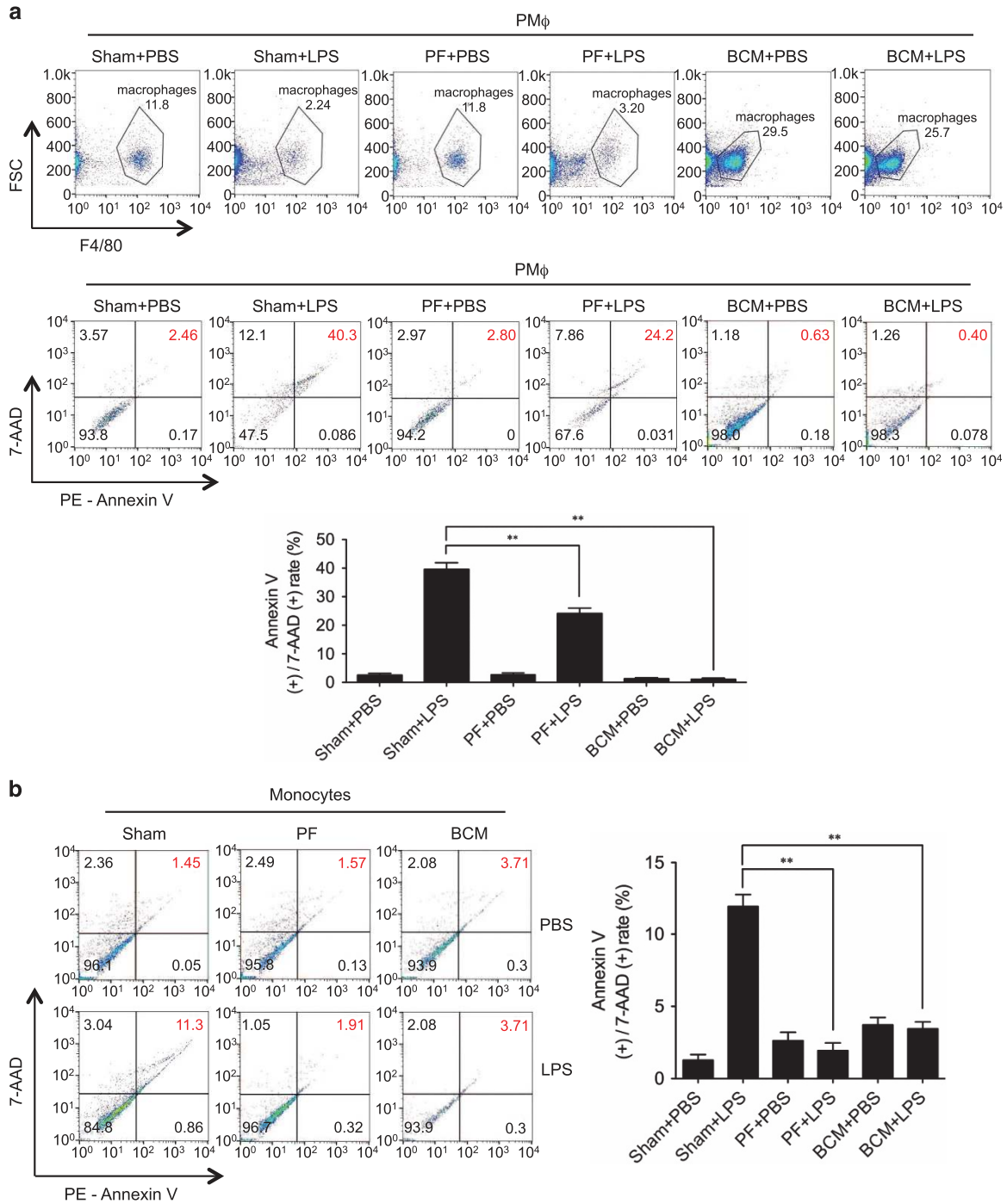


**Figure 1** Tissue damage suppresses LPS-induced monocytes/M $\phi$  necroptosis. WT mice were subjected to one of the following six groups: (1) Sham for 12 h followed by PBS (vehicle) 0.2 ml i.p. (Sham+PBS); (2) Sham for 12 h followed by LPS 2 mg/kg BW in 0.2 ml of PBS i.p. for 6 h (Sham+LPS); (3) Pseudo-fracture (PF) for 12 h followed by PBS 0.2 ml i.p. (PF+PBS); and (4) PF for 12 h followed by LPS 2 mg/kg BW i.p. in 0.2 ml of PBS for 6 h (PF+LPS); (5) 0.15 ml bone-crush mixture (BCM) i.p. for 12 h followed by PBS 0.2 ml i.p. (BCM+PBS); and (6) 0.15 ml BCM i.p. for 12 h followed by LPS 2 mg/kg BW i.p. in 0.2 ml of PBS for 6 h (BCM+LPS). (a and b) Peritoneal M $\phi$  (PM $\phi$ ) (a) and monocytes (b) were gated by F4/80 and double stained with PE-Annexin V and 7-AAD and analyzed by flow cytometer to calculate the cell death rate. (c and d) Peritoneal M $\phi$  (PM $\phi$ ) (c) and monocytes (d) were double stained with CD43 and Ly6C and analyzed by flow cytometer. (e) Confocal microscopy shows colocalization of RIPK1 (green) and RIPK3 (red) in PM $\phi$ , indicating necrosome formation. (f) BMDM were pretreated with or without 40  $\mu$ l/ml of BCM for 12 h and then LPS (1  $\mu$ g/ml) for 0–24 h. The cells were double stained with PE-Annexin V and 7-AAD and analyzed by flow cytometer to calculate the cell death rate. (g) BMDM were treated with 40  $\mu$ l/ml of BCM for 12 h and then with or without LPS (1  $\mu$ g/ml) for 6 h. In some groups, necrostatin-1 (Nec-1 s) (30  $\mu$ M), Ferrostatin-1 (Fer-1) (20  $\mu$ M), or z-VAD-FMK (25  $\mu$ M) was added into the BMDM. The cells were double stained with PE-Annexin V and 7-AAD and analyzed by flow cytometer to calculate the cell death rate. (h and i) WT BMDM were treated with BCM (40  $\mu$ l/ml) for 12 h, followed by 1  $\mu$ l/ml LPS for 6 h. RIPK1-RIPK3 binding in the BMDM was detected using co-immunoprecipitation and immunoblotting (h) and confocal microscopy (i). (j and k) Western blots show RIPK1 phosphorylation (j) and MLKL phosphorylation (k) in BMDM in response to the treatments of BCM for 12 h and/or LPS (1  $\mu$ g/ml) for 6 h. All results are representative of three independent experiments. The graphs show the mean and S.E.M.,  $n = 3$ . \* $P < 0.05$  compares between the indicated groups. \*\* $P < 0.01$  compares between the indicated groups. NS: no significant difference

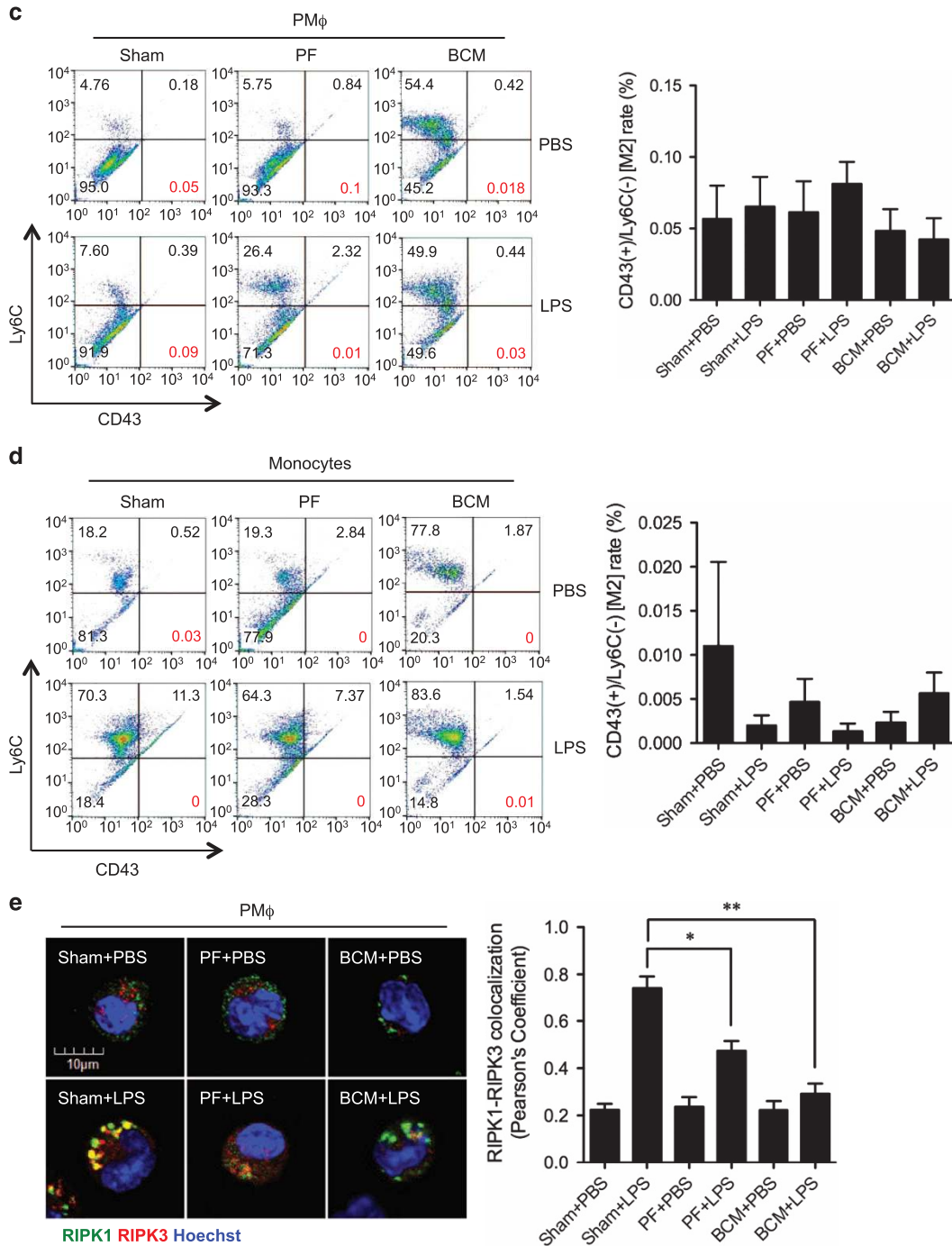


Figure 1 Continued

ligands is linked to a range of signaling pathways including activation of NF- $\kappa$ B,<sup>12</sup> PI3K/Akt,<sup>13</sup> mitogen activated protein kinases (MAPKs),<sup>14</sup> Jak/STAT,<sup>15</sup> Rho GTPases,<sup>16</sup> and Cell division control protein 42 homolog, also known as Cdc42,<sup>17</sup> although how RAGE transduces these signals is not yet fully understood.

TLR4 internalization has been reported as one of the mechanisms regulating a cell's responses to TLR4 signaling.<sup>18,19</sup> Mechanisms of TLR4 internalization can include association with endocytosis proteins such as clathrin,

dynamins, and caveolin-1.<sup>20,21</sup> Caveolin-1 is a transmembrane-scaffolding protein, and the major structural component of caveolae that contribute to many cell functions including endocytosis, potocytosis, transcytosis, as well as calcium signaling.<sup>21</sup> Caveolin-1-mediated internalization of multiple cell surface receptors is also known to critically regulate receptor signaling.<sup>22</sup>

In this study, we investigated the mechanisms and role of trauma/tissue damage in the regulation of LPS-induced M $\phi$  necroptosis using a validated mouse model that simulates

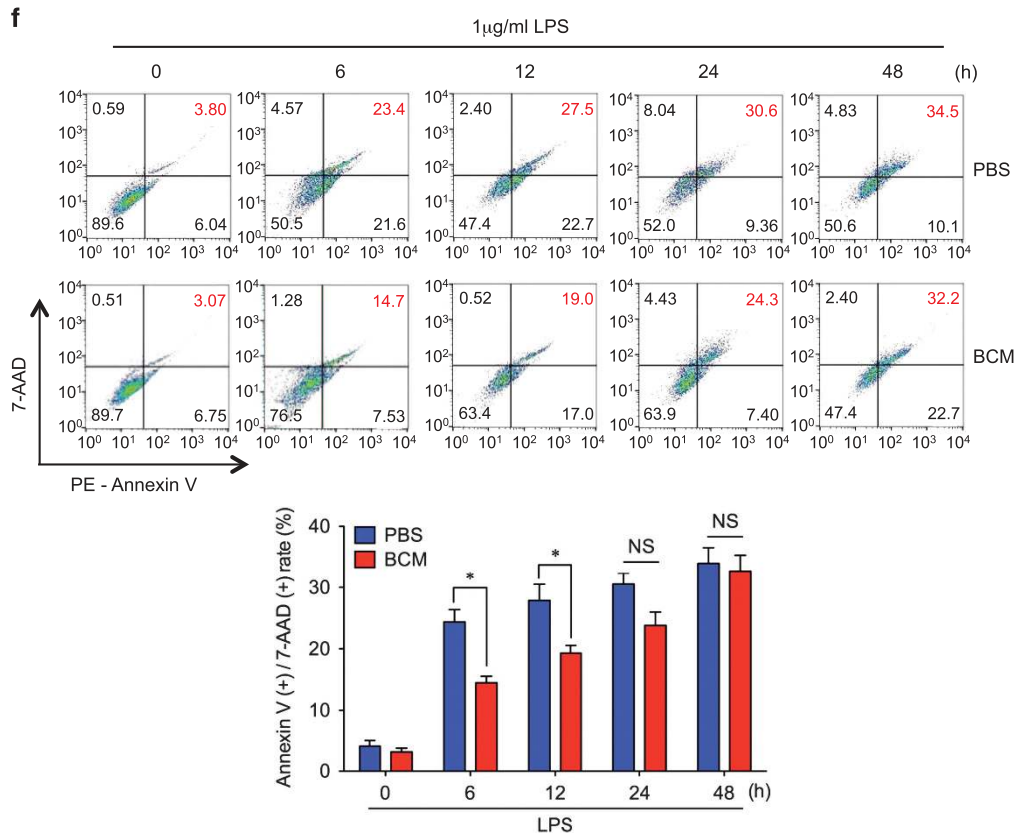


**Figure 1** Continued

long-bone fracture (pseudo-fracture; PF).<sup>23,24</sup> We demonstrate that LPS acting through TLR4 promotes M $\phi$  necroptosis, as expected. However, release of HMGB1 from damaged tissue signals via RAGE signaling to upregulate caveolin-1 expression and so induces M $\phi$  surface TLR4 internalization, which results in amelioration of LPS-TLR4-induced M $\phi$  necroptosis. We also identify a mechanism for upregulation of caveolin-1 expression via RAGE-MyD88 signaling to activate Cdc42, which leads to nuclear translocation of transcription factor Sp1 and subsequent change in caveolin-1 expression. These results reveal a previously unexplored negative regulatory effect of tissue damage on M $\phi$  response to a secondary LPS stimulation.

## Results

**Tissue damage suppresses LPS-induced monocytes/M $\phi$  necroptosis.** To determine M $\phi$  death response to post-trauma infection, wild-type (WT) mice were first subjected to PF, a validated model of long-bone fracture.<sup>23,24</sup> This model recapitulates both of the early and late immune responses seen after soft-tissue trauma with bone fracture, but as there is no fracture the mice can be assessed over longer time periods and do not have to be kept anesthetized for the entire study period. In the PF model 0.15 ml of bone-crush mixture (BCM) prepared from donor mouse femurs and tibias in sterile phosphate-buffer solution (PBS) is injected into the

thighs of recipient mice that also receive a soft-tissue crush injury.<sup>25</sup> At 12 h after PF, LPS was administered (2 mg/kg BW, i.p.), and peritoneal M $\phi$  (PM $\phi$ ) and peripheral monocytes were collected at 6 h after LPS for assessment of cell death, as defined by flow cytometry double-positive staining with 7-AAD and Annexin V. As shown in Figures 1a and b, although PF did not significantly alter M $\phi$ /monocyte death, antecedent PF markedly attenuated LPS-induced M $\phi$ /monocytes death.

To define the subtypes of the M $\phi$ /monocytes, the cells were also stained with Ly6C and CD43, the representative markers for M1 and M2 type of M $\phi$ /monocytes, respectively. As shown in Figures 1c and d, LPS and BCM did not cause a subtype transfer in the M $\phi$ /monocytes in the experimental settings.

To further confirm that necroptosis was occurring in the M $\phi$ /monocytes, cells were double stained with the RIPK1 and RIPK3.<sup>26</sup> Colocalization of RIPK1 and RIPK3 was visualized by confocal microscopy and represents the RIPK1 and RIPK3 association to form the necrosome.<sup>27</sup> Figure 1e shows that LPS induced necrosome formation, and prior PF decreased necrosome formation in PM $\phi$ .

To determine whether mediators in BCM contribute to the negative effect of PF on LPS-induced M $\phi$ /monocyte necroptosis, BCM (6 ml/kg BW) was directly injected into mouse peritoneum followed at 12 h by i.p. LPS (2 mg/kg BW). Necroptosis of PM $\phi$  and peripheral monocytes were assessed by flow cytometry at 6 h as described above. As shown in Figures 1a and b, BCM significantly decreased



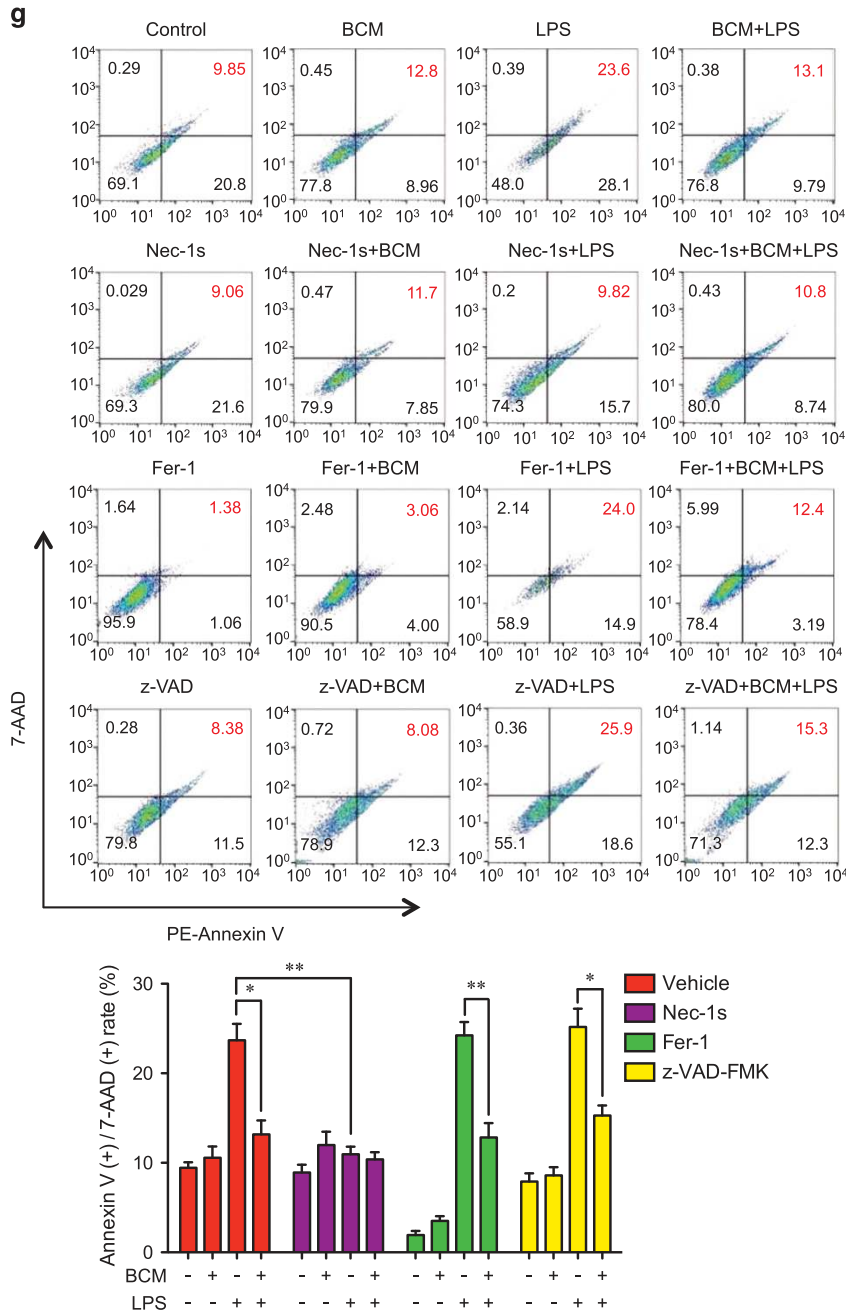


Figure 1 Continued

PM $\phi$ /monocytes necroptosis in response to LPS. BCM did not cause PM $\phi$ /monocytes subtype transferring as well (Figures 1c and d). Figure 1e shows that BCM pretreatment similarly diminished LPS-induced necrosome formation in PM $\phi$ . These results suggest that mediators within BCM are responsible for the PF suppression of M $\phi$  necroptosis in response to LPS.

The *in vivo* study was also recapitulated *in vitro*. Bone marrow-derived macrophage (BMDM) were treated with BCM (40  $\mu$ l/ml) for 12 h, followed by withdrawal of BCM, addition of LPS (1  $\mu$ l/ml) and continuous incubation for an additional 48 h.

As shown in Figure 1f, macrophage necroptosis had increased by 48 h after BCM withdrawal.

To further confirm the type of the M $\phi$  death induced by LPS, BMDM were pretreated with necroptosis inhibitor necrostatin-1 s<sup>28</sup> (Nec-1s) (30  $\mu$ M), ferroptosis inhibitor ferrostatin-1 (Fer-1) (20  $\mu$ M), or pan-caspase inhibitor z-VAD-FMK<sup>29</sup> (25  $\mu$ M) for 10 min before incubation with BCM (40  $\mu$ l/ml) for 12 h and subsequent LPS stimulation (1  $\mu$ g/ml) for an additional 6 h. As shown in Figure 1g, Nec-1 s prevented LPS-induced cell death, and BCM failed to further decrease the LPS-induced cell death in Nec-1 s pretreated groups; in

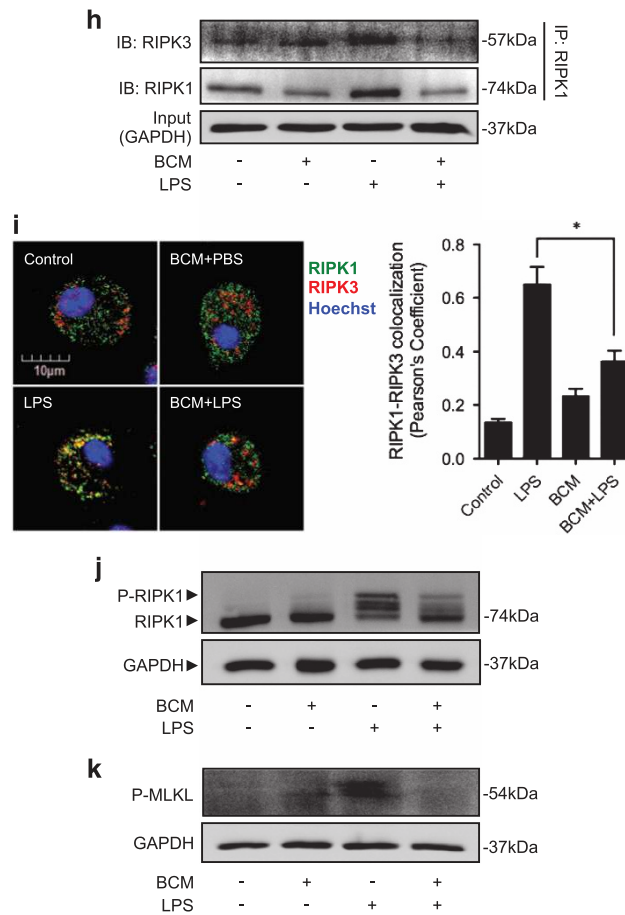


Figure 1 Continued

contrast, Fer-1 and z-VAD-FMK did not significantly decrease LPS-induced cell death. Furthermore, immunoblotting and confocal microscopy show that LPS-induced association of RIPK1 and RIPK3 (Figures 1h and i) and phosphorylation of RIPK1<sup>30,31</sup> (Figure 1j) and MLKL (Figure 1k) in BMDM were also attenuated with BCM treatment.

Collectively, these results suggest that the portion of M $\phi$  death induced by LPS and suppressed by damaged tissue is mainly necroptosis, and BCM is responsible for the negative effect of PF on LPS-induced M $\phi$  necroptosis.

**BCM decreases cell surface expression of TLR4.** TLR4 is the cell surface receptor for LPS.<sup>32,33</sup> To address whether BCM suppresses LPS-induced M $\phi$  necroptosis by altering TLR4 expression, we measured M $\phi$  surface expression of TLR4. Although incubation of BMDM with BCM (40  $\mu$ l/ml) for 0–24 h did not alter total TLR4 protein expression in the BMDM (Figure 2a), BCM promoted TLR4 translocation from cell surface into cytoplasm by 12 h after BCM treatment (Figure 2b). Flow cytometry also showed that BCM decreased TLR4 cell surface expression on BMDM by ~64% at 12 h as compared with the group treated with no BCM (time = 0; Figure 2c). These results indicate that BCM decreases M $\phi$  surface TLR4 expression by inducing TLR4 internalization.

To define a time-course change in BCM-induced TLR4 internalization, BMDM were treated with BCM for 12 h followed by withdrawing of BCM and continuous incubation for additional 48 h. Flow cytometry (Figure 2d) and confocal microscopy (Figure 2e) show that TLR4 surface expression started to restore during the time between 12 h and 24 h after BCM withdrawing.

**HMGB1-RAGE signaling mediates BCM-suppressed M $\phi$  necroptosis in response to LPS.** HMGB1 has been reported as a major DAMP released during trauma<sup>34</sup> and presents at a high concentration in bone marrow.<sup>35</sup> To address whether HMGB1 mediates tissue damage-suppression of M $\phi$  necroptosis in response to LPS, we prepared HMGB1-deficient BCM from femurs and tibias harvested from inducible HMGB1-knockout mice<sup>36</sup> (Figure 3a), and used the HMGB1-deficient BCM to treat BMDM. We found that HMGB1-deficient BCM failed to reduce LPS-induced BMDM necroptosis (Figure 3b), RIPK1 phosphorylation (Figure 3c), and RIPK1-RIPK3 binding (Figure 3d), as well as failed to induce TLR4 internalization and decrease cell surface expression of TLR4 (Figures 3e and f).

To further confirm the role of HMGB1 in suppressing M $\phi$  necroptosis in response to LPS, BMDM were pretreated with recombinant HMGB1 for 12 h followed by LPS stimulation for

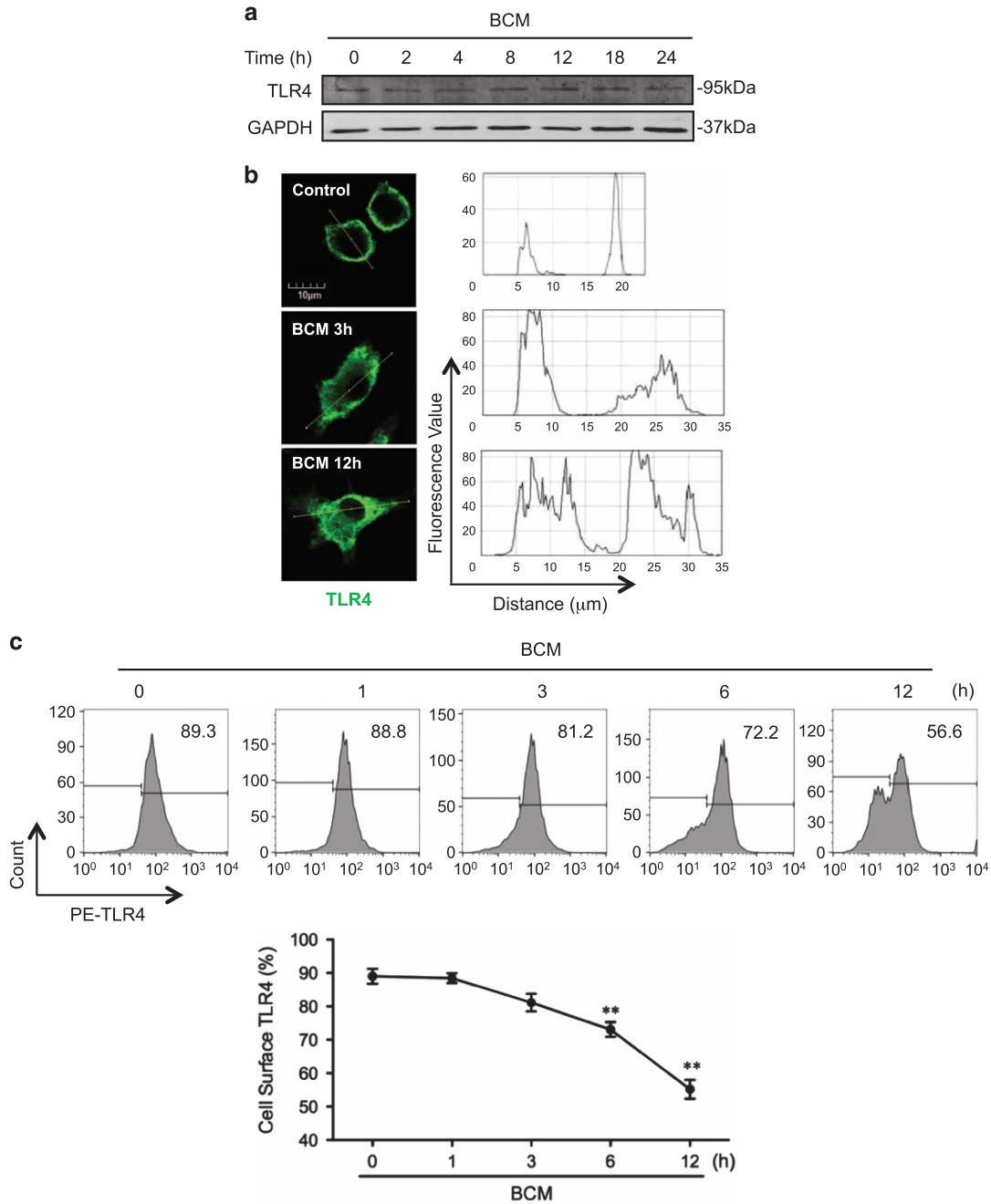


**Figure 2** BCM decreases cell surface expression of TLR4. (a) Western blot showing the total TLR4 expression in BMDM whole-cell lysate, which was challenged with 40  $\mu$ l/ml BCM for 0–24 h. (b) Immunofluorescence images showing the TLR4 localization and fluorescence distribution in BMDM, which were stimulated with BCM (40  $\mu$ l/ml) for 3 and 12 h, respectively. (c) Flow cytometry showing the cell surface TLR4 expression on BMDM, which were stimulated with BCM (40  $\mu$ l/ml) for 0–12 h and stained with PE-tagged anti-TLR4 antibody. (d and e) BMDM were stimulated with BCM (40  $\mu$ l/ml) for 12 h followed by withdrawing BCM and continuous incubation in normal medium for 0–48 h. The cell surface TLR4 was then stained with PE-tagged anti-TLR4 antibody and detected by flow cytometry (d) and visualized by confocal microscopy using fluorescent-tagged TLR4 antibody (e). All results are representative of three independent experiments. The graph shows the mean and S.E.M.,  $n=3$ . \* $P<0.05$  and \*\* $P<0.01$  versus the control

an additional 6 h. As shown in Figure 3b, HMGB1 decreased LPS-induced BMDM necroptosis by ~50%. These data indicate that HMGB1 is a major component in BCM-mediated tissue damage-suppressed necroptosis induced by LPS.

RAGE is one of the known receptors for HMGB1.<sup>37</sup> Using BMDM isolated from RAGE<sup>-/-</sup> mice, we found that the effects of BCM on TLR4 internalization and LPS-induced M $\phi$

necroptosis completely disappeared in the RAGE<sup>-/-</sup> BMDM compared with WT BMDM (Figures 3g–j). These results indicate that HMGB1-RAGE signaling is required for the BCM-mediated negative regulation of LPS-induced M $\phi$  necroptosis.

**Caveolin-1 mediates RAGE-TLR4 interaction.** Caveolin-1 has an important role in caveolae-mediated receptor

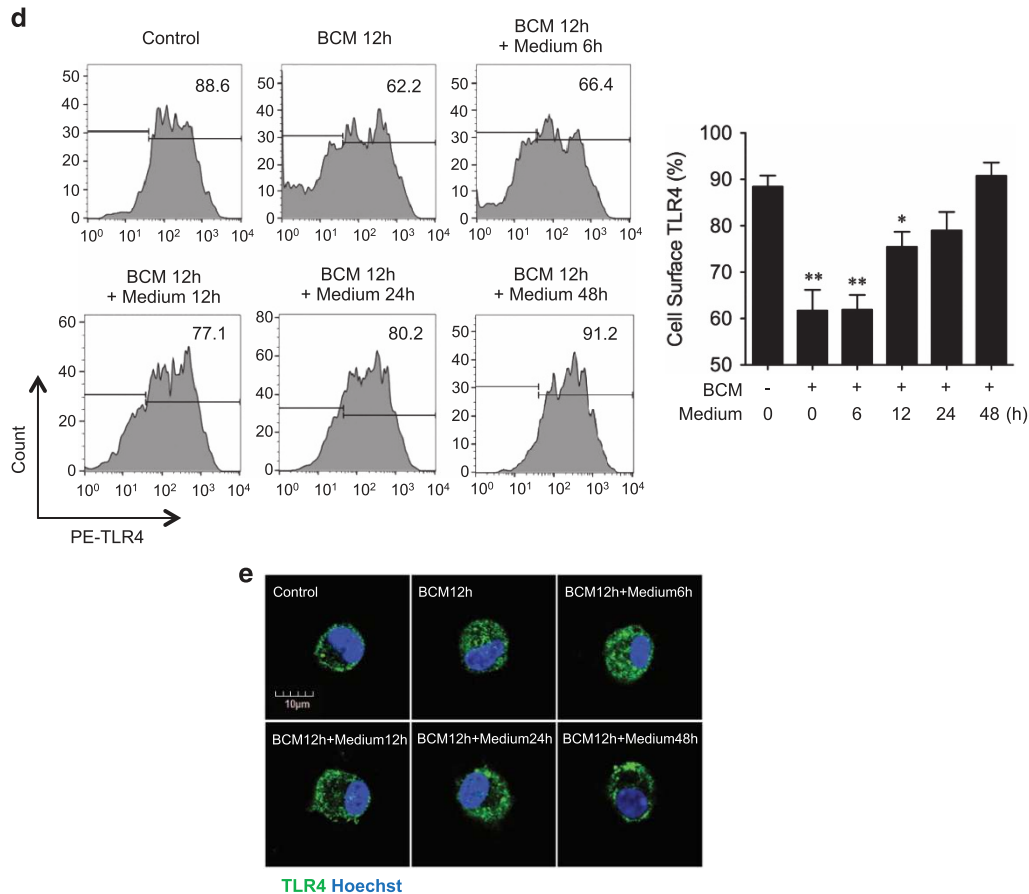


**Figure 2** Continued

internalization and desensitization, which includes regulating TLR4 signaling.<sup>38</sup> To determine the role of caveolin-1 in RAGE signaling-induced TLR4 internalization, we first measured caveolin-1 expression in BMDM treated with BCM for up to 24 h. We found that in WT BMDM, BCM treatment increased caveolin-1 mRNA expression by 6 h and was increased by ninefold at 24 h. However, BCM failed to upregulate caveolin-1 mRNA expression in RAGE<sup>-/-</sup> BMDM (Figure 4a). Consistent with the changes in mRNA, BCM increased caveolin-1 protein expression in WT BMDM, but not in RAGE<sup>-/-</sup> BMDM (Figure 4b). In addition, the HMGB1-deficient BCM failed to induce the caveolin-1 mRNA and protein expression in WT BMDM by 12 h (Figures 4c and e), and stimulation of WT BMDM with recombinant HMGB1 for 12 h increased caveolin-1 mRNA and protein expression (Figures 4c and d). Next, we treated cells with filipin (20 μM, add 20 min before treatment), a caveolin-1 inhibitor, to test the role of caveolin-1 in inducing TLR4 internalization. As shown in Figure 4f, filipin prevented BCM-induced TLR4 internalization. Furthermore, confocal microscopy demonstrated a colocalization of caveolin-1 and TLR4 near the plasma membrane in WT BMDM, but not in RAGE<sup>-/-</sup> BMDM, starting at 8 h after BCM treatment (Figure 4g). This BCM-induced colocalization of caveolin-1 and TLR4 in WT BMDM was blocked by filipin as well (Figure 4h).

The *in vitro* findings were also observed *in vivo*. PF or direct peritoneal injection of BCM resulted in the binding of caveolin-1 and TLR4 (Figure 4i) and decrease in cell surface TLR4 expression (Figure 4j) in PMφ at 12 h after the treatment.

Taken together, these data suggest an important role of caveolin-1 in mediating RAGE signaling-induced TLR4 internalization.

**RAGE-MyD88 signaling mediates translocation of Sp1 to upregulate caveolin-1 expression.** Previous studies have reported that transcription factor Sp1 regulates caveolin-1 gene expression.<sup>39</sup> We thus hypothesized that RAGE signaling acting through Sp1 upregulates caveolin-1 expression, which then promotes caveolae-mediated TLR4 internalization.

To test this hypothesis, we first determined the role of Sp1 in upregulation of caveolin-1. Pretreatment of WT BMDM with mithramycin A, a specific Sp1 inhibitor,<sup>40,41</sup> prevented BCM-induced expression of caveolin-1 mRNA and protein (Figures 5a and b), as well as BCM reduced Mφ surface expression of TLR4, a reflection of TLR4 internalization (Figure 5c).

Next, we addressed whether BCM is able to induce nuclear translocation of Sp1. By immunofluorescently staining Sp1, we observed nuclear translocation of Sp1 in WT BMDM starting at 6 h after the BCM treatment (Figure 5d). However,



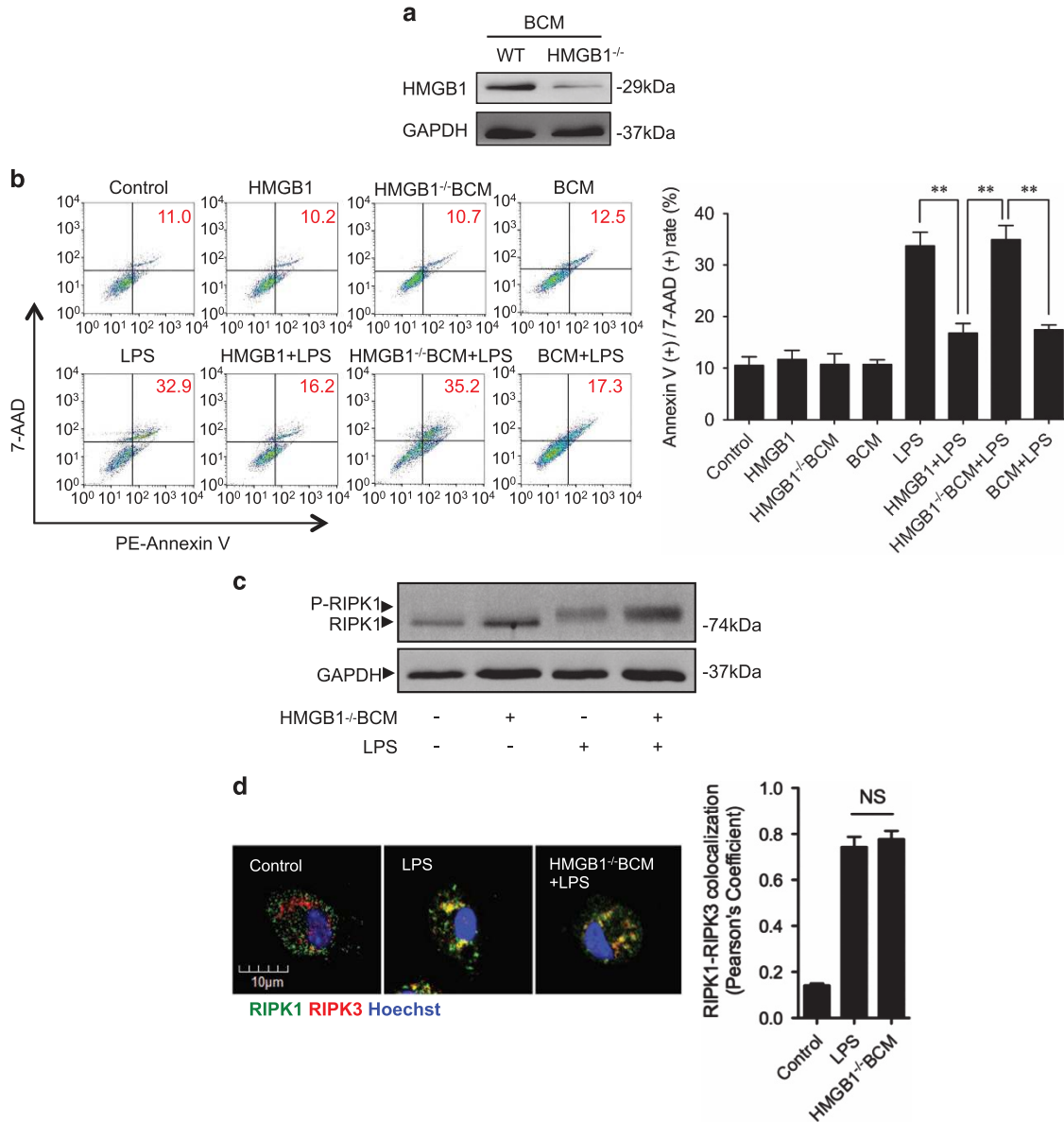


**Figure 3** HMGB1-RAGE signal mediates BCM-suppressed Mφ necroptosis in response to LPS. (a) Western blot showing the HMGB1 expression in WT and HMGB1-lacking BCM. (b) WT BMDM were pretreated with 0.3 μg/ml HMGB1 or 40 μl/ml HMGB1-lacking BCM or 40 μl/ml WT BCM for 12 h, followed by challenge of LPS (1 μg/ml) or PBS for 6 h. Cells were double stained with PE-Annexin V and 7-AAD. Cell death rates were analyzed by flow cytometry. (c) Western blot showing RIPK1 phosphorylation in BMDM in response to the treatments of HMGB1-deficient BCM for 12 h and/or LPS (1 μg/ml) for 6 h. (d) Immunofluorescence images showing the colocalization of RIPK1 and RIPK3, which refers to necrosomes formation in the BMDM pretreated with or without 40 μl/ml of HMGB1-lacking BCM for 12 h followed by challenge of LPS (1 μg/ml) for 6 h. (e) Immunofluorescence with confocal microscopy showing the distribution of TLR4 in BMDM, which were stimulated with WT or HMGB1-lacking BCM for 12 h. (f) Flow cytometry showing the cell surface TLR4 expression on BMDM, which were stimulated with 40 μl/ml WT or HMGB1-lacking BCM for 12 h and stained with PE-tagged anti-TLR4 antibody. (g) Western blot showing TLR4 expression in RAGE<sup>-/-</sup> BMDM, which were challenged with 40 μl/ml BCM for 0–12 h. (h) Immunofluorescence images showing the TLR4 localization and distribution in RAGE<sup>-/-</sup> BMDM, which were stimulated of BCM for 3 or 12 h and stained with PE-tagged anti-TLR4 antibody. (i) Flow cytometry showing the cell surface TLR4 expression on RAGE<sup>-/-</sup> BMDM, which were stimulated with 40 μl/ml BCM for 0–12 h and stained with PE-tagged anti-TLR4 antibody. (j) RAGE<sup>-/-</sup> BMDM were pretreated with 40 μl/ml BCM for 12 h and then were cultured with PBS (BCM+PBS) or 1 μg/ml LPS (BCM+LPS) for additional 6 h. The cells death rates were analyzed by flow cytometry. All results are representative of three independent experiments. The graphs show the mean and S.E.M., n = 3. \*\*P < 0.01 compares between the indicated groups. NS: no significant difference

BCM failed to induce the Sp1 nuclear translocation in RAGE<sup>-/-</sup> BMDM (Figure 5d). Similarly, HMGB1-deficient BCM, prepared as above from HMGB1 conditional KO mice, also failed to induce Sp1 nuclear translocation in WT BMDM (Figure 5d).

Furthermore, to identify the intracellular signaling that induces Sp1 activation, we screened proteins that associate with RAGE in BMDM after BCM stimulation. Using immunoprecipitation and immunoblotting, we found that RAGE coprecipitated with MyD88 starting at 6 h after BCM treatment

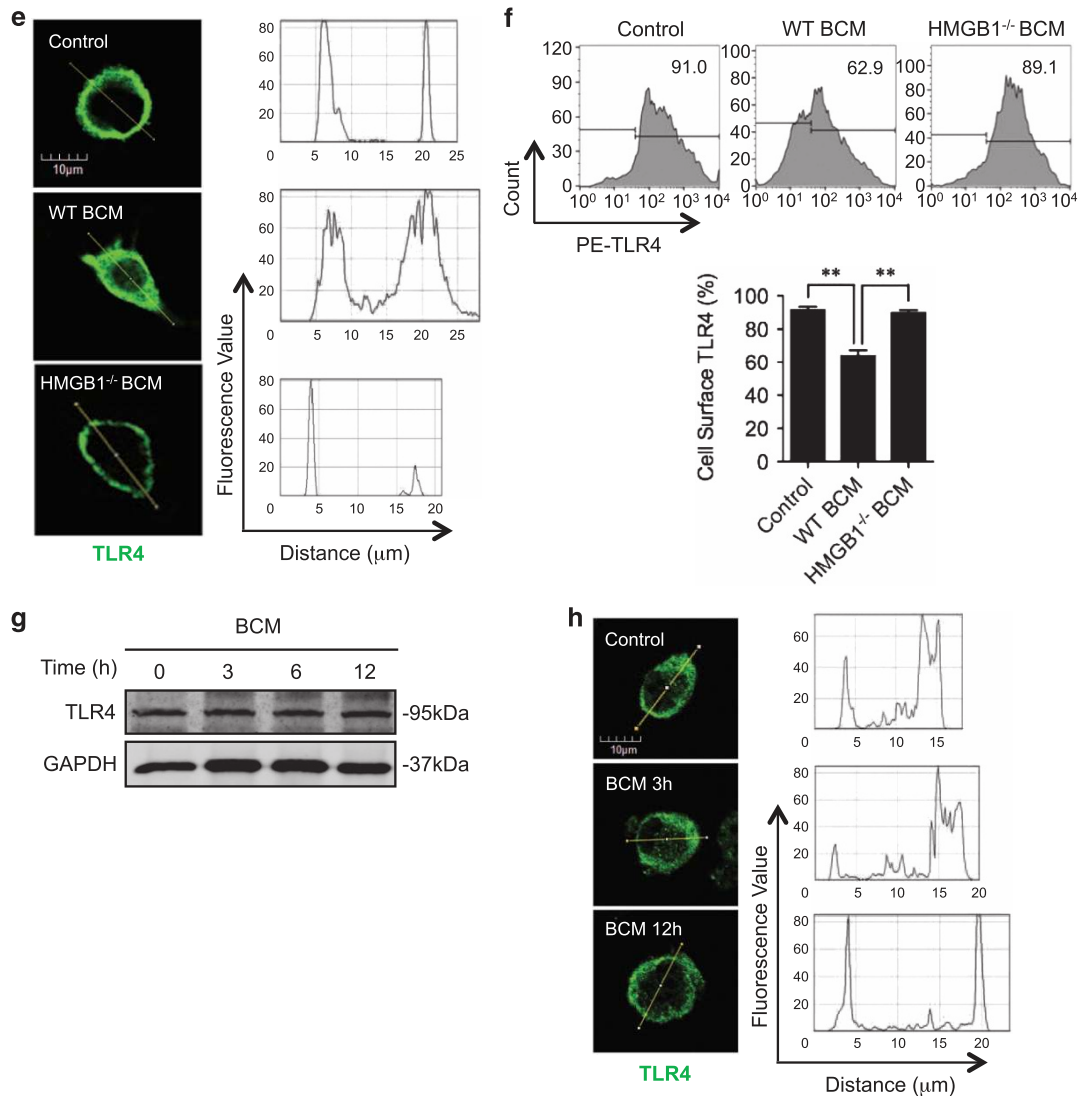


**Figure 3** Continued

(Figure 5e). We further confirmed the role of MyD88 in upregulation of caveolin-1 using MyD88<sup>-/-</sup> BMDM. MyD88-deficiency prevented BCM-induced expression of caveolin-1 mRNA (Figure 5f) and protein (Figure 5g), and this role for MyD88 seemed to be independent of TLR4 signaling, as TLR4-deficiency (TLR4<sup>-/-</sup> BMDM) had no effect on BCM-induced caveolin-1 protein expression measured by western blot (Figure 5g), or visualized by confocal microscopy (Figure 5h). In addition, in MyD88<sup>-/-</sup> BMDM, BCM failed to induce Sp1 nuclear translocation (Figure 5i) and TLR4 internalization (Figure 5j).

Finally, we investigated the role of cdc42 as a downstream signaling partner in the MyD88 signaling pathway by using cdc42-specific inhibitor ML141.<sup>42</sup> BMDM were pretreated with ML141 (35 μM) for 20 min followed by adding BCM and incubation for additional 12 h. ML141 significantly decreased the BCM-induced caveolin-1 mRNA expression (Figure 5k) and Sp1 nuclear translocation (Figure 5l).

Taken together, these findings support the hypothesis that HMGB1-RAGE-MyD88 signaling through the activation of Sp1 and upregulation of caveolin-1 induces caveolae-mediated TLR4 internalization in Mφ.

#### Tissue damage suppresses LPS-induced inflammation.

To address whether BCM-induced TLR4 internalization alleviates LPS-prompted inflammation, we subjected WT mice to PF for 12 h followed by LPS i.p., and at 6 h after LPS, measured IL-6 and TNFα levels in the mouse peritoneal lavage fluid and serum. As shown in Figure 6a, LPS caused markedly higher levels of IL-6 and TNFα in both lavage fluid and serum, as expected. However, antecedent PF significantly decreased subsequent LPS-induced secretion of IL-6 and TNFα (Figure 6a).

To determine the role of cell necroptosis in enhancing inflammatory cytokines release, we injected WT mice with Nec-1 s (30 mmol/kg BW, i.p.) combined with LPS or saline for 6 h. As shown in Figure 6a, inhibition of necroptosis

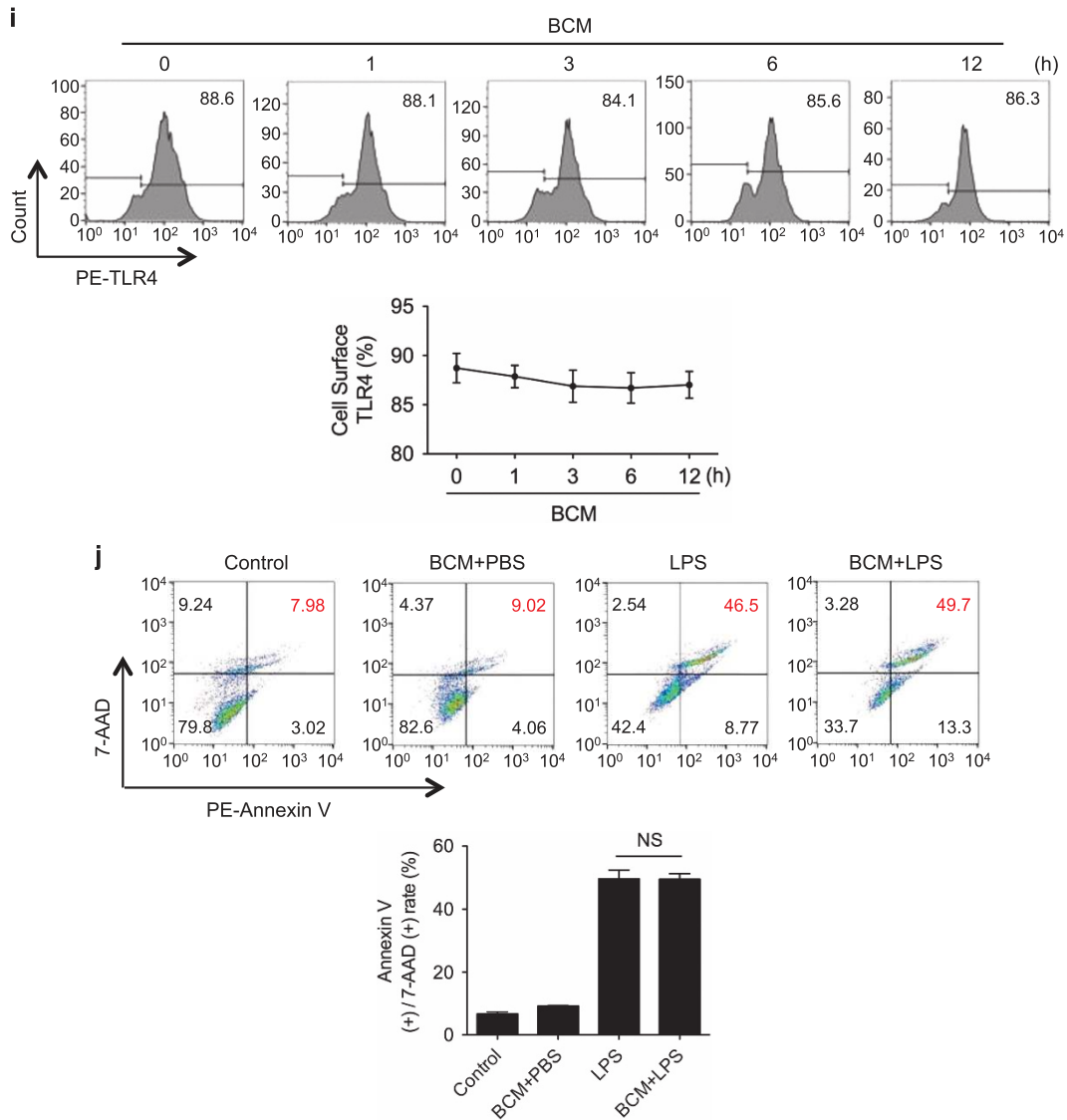


**Figure 3** Continued

significantly decreased LPS-induced release of IL-6 and TNF $\alpha$  in peritoneal lavage fluid and serum.

Activation of MAPK, which includes p38 and ERK1/2, is also an important response to LPS,<sup>43</sup> and subsequently induces phosphorylation and activation of numerous transcription factors that promote inflammatory mediators synthesis and release.<sup>44</sup> We observed that LPS-activated p38 and ERK1/2 phosphorylation in BMDM peaked at 0.5 h after LPS stimulation (Figure 6b). Pretreatment of BMDM with BCM for 12 h diminished the LPS-induced phosphorylation of p38 and ERK1/2 (Figure 6c). In RAGE<sup>-/-</sup> BMDM, BCM pretreatment failed to decrease LPS-induced phosphorylation of p38 and ERK1/2 (Figure 6d), or decrease IL-6 and TNF $\alpha$  concentrations in cell culture medium (Figure 6e), as compared with WT BMDM. Furthermore, pretreatment of WT BMDM with HMGB1-deficient BCM for 12 h was not able to suppress LPS-induced phosphorylation of p38 and ERK1/2 (Figure 6f) and to decrease the levels of IL-6 and TNF $\alpha$  in the cell culture

medium (Figure 6g). These results further demonstrated the negative regulatory effect of BCM/RAGE signaling on M $\phi$  response to LPS.

## Discussion

Tissue damage resulting from major surgery and severe trauma frequently combines with infection or renders the patients more susceptible to infection. The interaction between tissue damage and infection is believed an important determinant regulating the progress of the host's inflammatory response. Our previous studies and those of others have shown that trauma-induced release of DAMPs serves as a priming factor, which often enhances inflammatory responses to infection and bacterial products.<sup>45-50</sup> Those results, therefore, suggested that blocking DAMP-signaling may attenuate inflammatory responses to a secondary infection. In the current study, however, we demonstrate a novel finding that

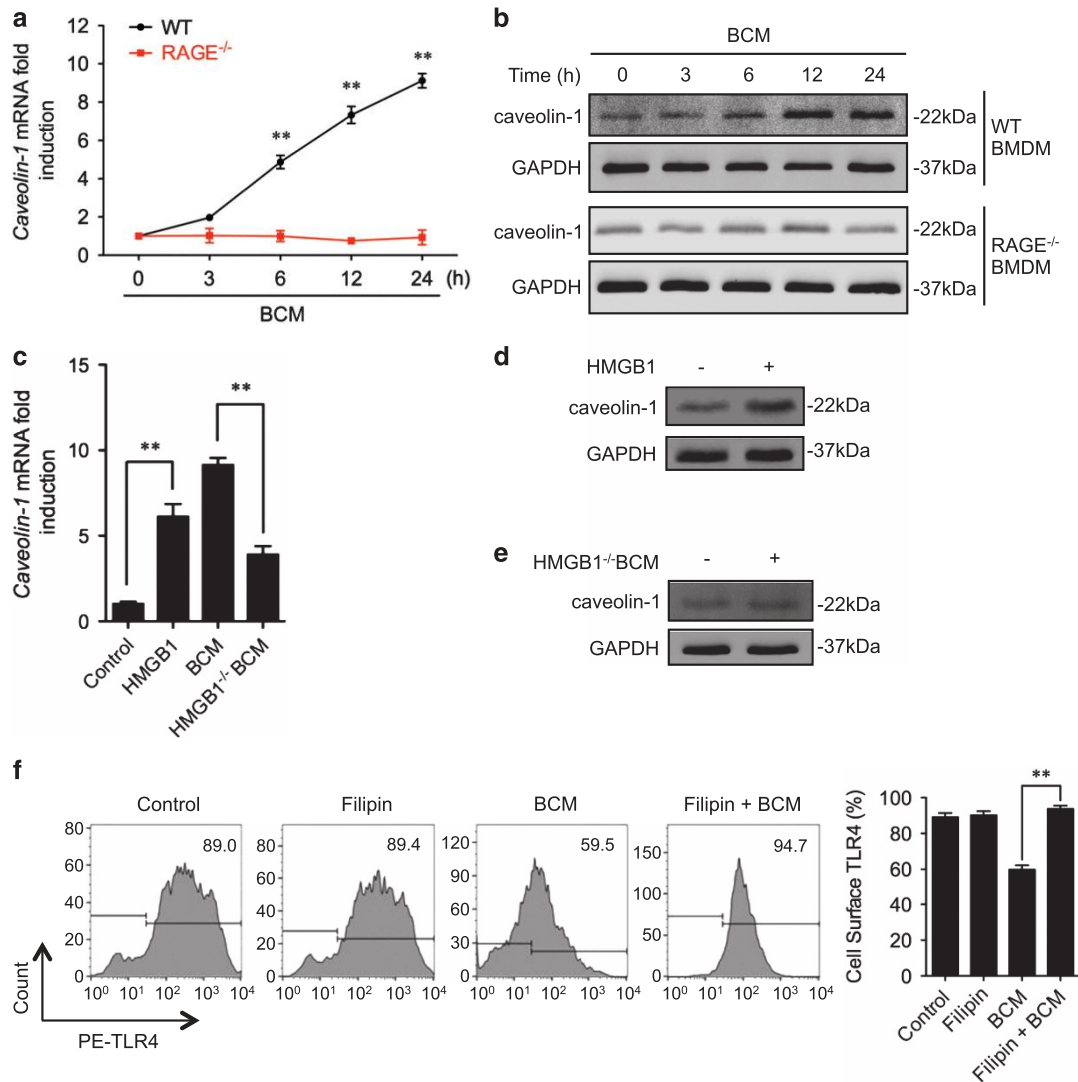


**Figure 4** Caveolin-1 mediates RAGE-TLR4 interaction. (a and b) WT or RAGE<sup>-/-</sup> BMDM were stimulated by 40  $\mu$ l/ml of BCM for 0–24 h, and caveolin-1 mRNA (a) and protein (b) in the BMDM were measured by Q-RT-PCR and western blot. (c) WT BMDM were pretreated with 0.3  $\mu$ g/ml recombinant HMGB1 or 40  $\mu$ l/ml HMGB1-deficient BCM for 12 h, followed by challenge of LPS (1  $\mu$ g/ml) or PBS for 6 h. The caveolin-1 mRNA in the BMDM was measured by QRT-PCR. (d and e) Western blot showing the caveolin-1 expression after the treatment with 40  $\mu$ l/ml HMGB1-lacking BCM (d) or 0.3  $\mu$ g/ml recombinant HMGB1 (e) for 12 h. (f) BMDM were pretreated with or without 20  $\mu$ M of filipin, a caveolea inhibitor, followed by treatment of 40  $\mu$ l/ml BCM for 12 h. The cell surface expression of TLR4 was analyzed by flow cytometry. (g) Immunofluorescence images showing the colocalization of Caveolin-1 (green) and TLR4 (red) in WT and RAGE<sup>-/-</sup> BMDM after BCM treatment (40  $\mu$ l/ml) for 0–12 h. (h) Confocal microscopy showing the Caveolin-1 (green) and TLR4 (red) colocalization after treatment of BCM (40  $\mu$ l/ml) in the presence or absence of 20  $\mu$ M of filipin. (i) Peritoneal M $\phi$  (PM $\phi$ ), which were collected from the mice subjected to sham, pseudo-fracture, or BCM injection (0.15 ml, i.p.) at 12 h after the treatments, were double stained with caveolin-1 (green) and TLR4 (red), and the colocalization of caveolin-1 and TLR4 was detected by confocal microscopy. (j) Peritoneal M $\phi$  (PM $\phi$ ), which were collected from the mice subjected to sham, pseudo-fracture, or BCM injection (0.15 ml, i.p.) at 12 h after the treatments, were subjected to flow cytometry analysis for cell surface TLR4 using PE-tagged TLR4 antibody. The macrophages were defined by F4/80 positive. All results are representative of three independent experiments. The graphs show the mean and S.E.M.,  $n=3$ . \*\* $P<0.01$  compares between the indicated groups

tissue damage suppresses subsequent LPS-induced M $\phi$  necroptosis through DAMP signaling, thereby exhibits a negative regulatory effect on the inflammatory response to a secondary LPS stimulation. We show, as others have, that LPS acting through TLR4 promotes M $\phi$  necroptosis. However in the setting of trauma, release of HMGB1 by damaged tissue upregulates caveolin-1 expression in M $\phi$  via HMGB1/RAGE signaling, which in turn induces caveolae-mediated TLR4 internalization to reduce LPS-TLR4-induced M $\phi$  necroptosis.

Part of the mechanism for upregulation of caveolin-1 is through RAGE-MyD88 signaling and downstream activation of Cdc42, leading to nuclear translocation of transcription factor Sp1 and alteration of caveolin-1 expression (Figure 7). It seems clear that transcriptional upregulation of caveolin-1 is important in inducing TLR4 internalization; although posttranscriptional modification of caveolin-1, that is, tyr14 phosphorylation may also be needed.<sup>51</sup> Data from this study therefore suggest that DAMP molecules, in a defined period following

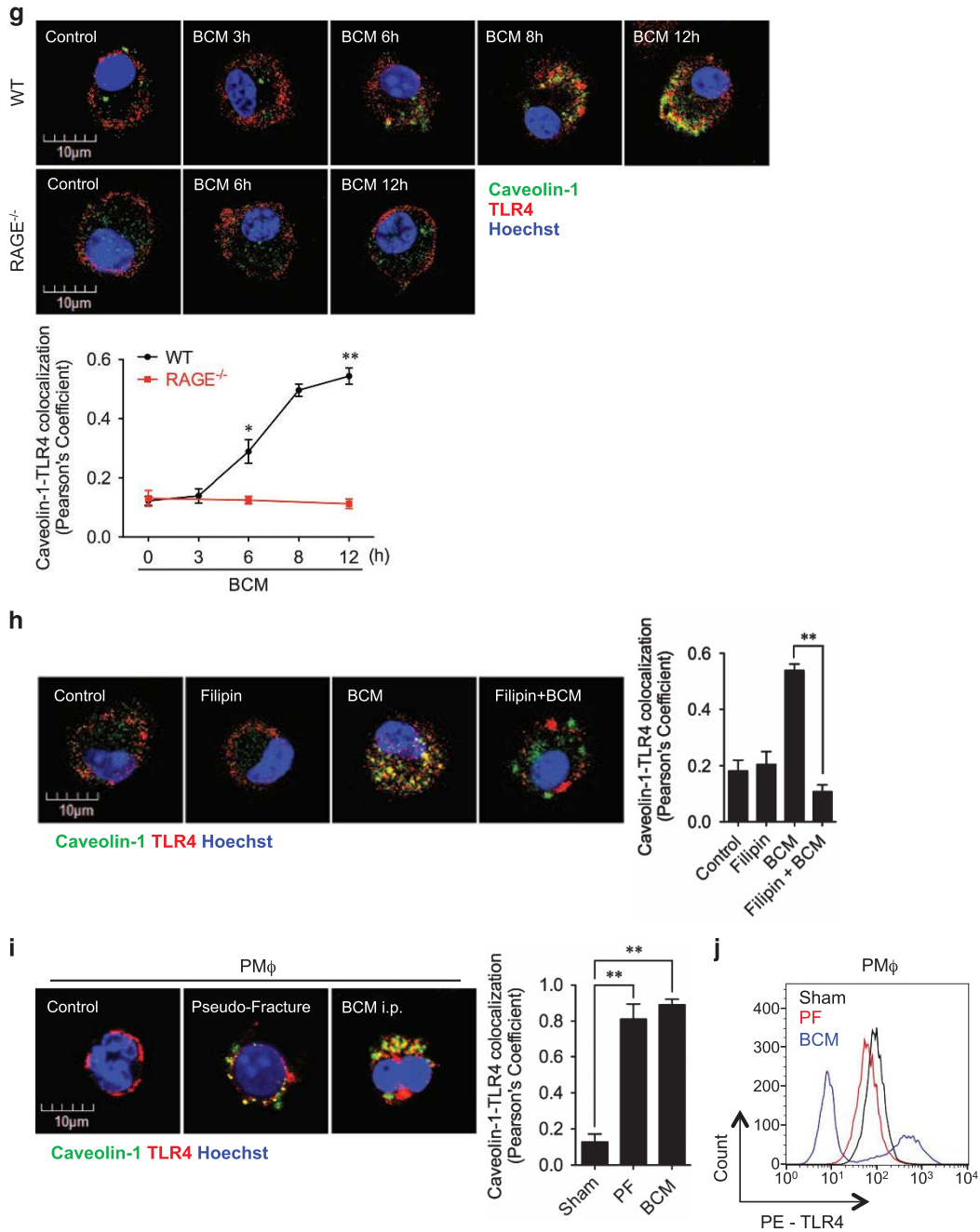


Figure 4 Continued

tissue damage, are not just pro-inflammatory but can also negatively regulate host inflammatory responses to LPS, as shown by our *in vivo* findings. This suggests that targeting DAMP molecules as a therapeutic strategy for post-trauma inflammation may need to take timing or potential treatments into consideration to avoid bad outcomes.

PF is a reproducible murine model of sterile musculoskeletal trauma that allows for evaluation of post-traumatic immune responses.<sup>24</sup> The challenges in experimental murine trauma modeling include technical difficulties in fracture fixation in mice and reproducibility. The PF model overcomes these

difficulties by immunologically mimicking an extremity fracture environment, whereas allowing freedom of movement in the animals and long-term survival without continual, prolonged use of anesthesia. The intent is to recreate the features of a long-bone fracture; injured muscle and soft tissue are exposed to damaged bone and bone marrow without breaking the native bone. The PF model consists of two parts: a muscle-crush injury to the hind limbs, followed by injection of a bone solution into these injured muscles.<sup>24</sup> In the current study, we used the PF model to elucidate the influence of tissue damage on LPS-induced Mφ necroptosis, and revealed that HMGB1



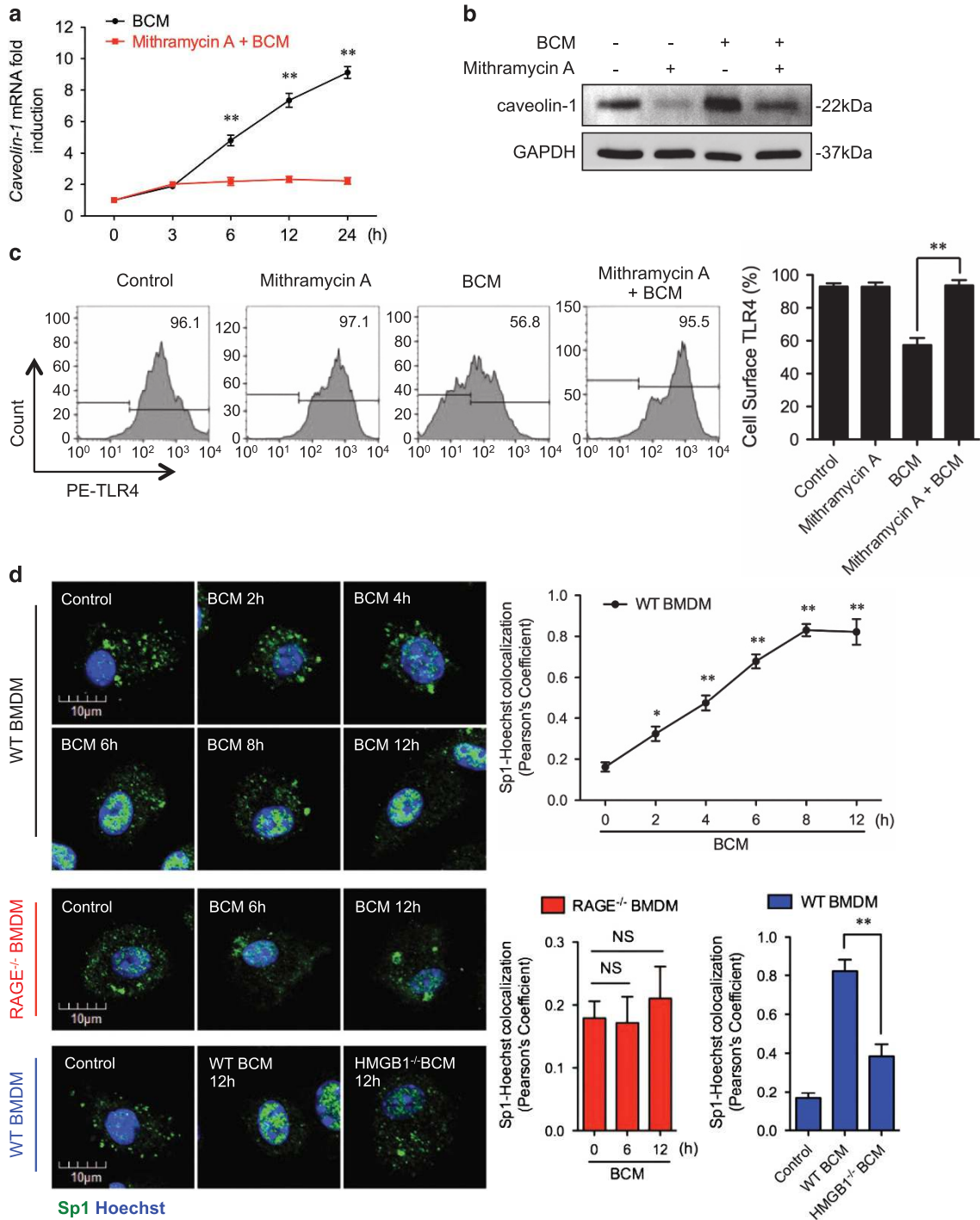


**Figure 5** RAGE-MyD88 signaling-activated Sp1 upregulates caveolin-1 expression. (a–c) BMDM were pretreated with or without 30  $\mu$ M of Mithramycin A, a Sp1-specific inhibitor, followed by treatment of 40  $\mu$ l/ml of BCM for 12 h. The caveolin-1 mRNA (a) and protein (b) expression as well as the cell surface TLR4 expression (c) were measured by QRT-PCR, western blot, and flow cytometry, respectively. (d) Immunofluorescence images showing the nuclear translocation of transcriptional factor Sp1 in WT and RAGE<sup>-/-</sup> BMDM following the treatment of WT or HMGB1-lacking BCM (40  $\mu$ l/ml) for 0–12 h. (e) WT BMDM were treated with BCM (40  $\mu$ l/ml) for 0–12 h. The BMDM were then recovered for the detection of RAGE-MyD88 binding using immunoprecipitation and immunoblotting. (f) WT and MyD88<sup>-/-</sup> BMDM were treated with BCM (40  $\mu$ l/ml) for 12 h. The caveolin-1 mRNA level in the BMDM was measured by QRT-PCR. (g) TLR4<sup>-/-</sup> or MyD88<sup>-/-</sup> BMDM were stimulated by BCM (40  $\mu$ l/ml) for 0–24 h, and the caveolin-1 protein expression in the BMDM was detected by western blot. (h) The images showing the Caveolin-1 (green) and TLR4 (red) localization in TLR4<sup>-/-</sup> BMDM and MyD88<sup>-/-</sup> BMDM treated with BCM (40  $\mu$ l/ml) for 6 and 12 h. (i) MyD88<sup>-/-</sup> BMDM were stimulated by BCM (40  $\mu$ l/ml) for 6 and 12 h, and the Sp1 (green) localization was visualized by confocal microscopy. (j) MyD88<sup>-/-</sup> BMDM were treated with BCM (40  $\mu$ l/ml) for 0–12 h, and the cell surface expression of TLR4 was detected by flow cytometry. (k and l) WT BMDM were treated with BCM (40  $\mu$ l/ml) for 12 h in the presence or absence of 35  $\mu$ M of ML141, an inhibitor of Cdc42. The caveolin-1 mRNA (k) and Sp1 nuclear translocation (l) were measured by Q-RT-PCR and confocal immunofluorescence microscopy, respectively. All results are representative of three independent experiments. The graphs show the mean and S.E.M.,  $n=3$ . \*\* $P<0.01$  versus the control or compares between the indicated groups

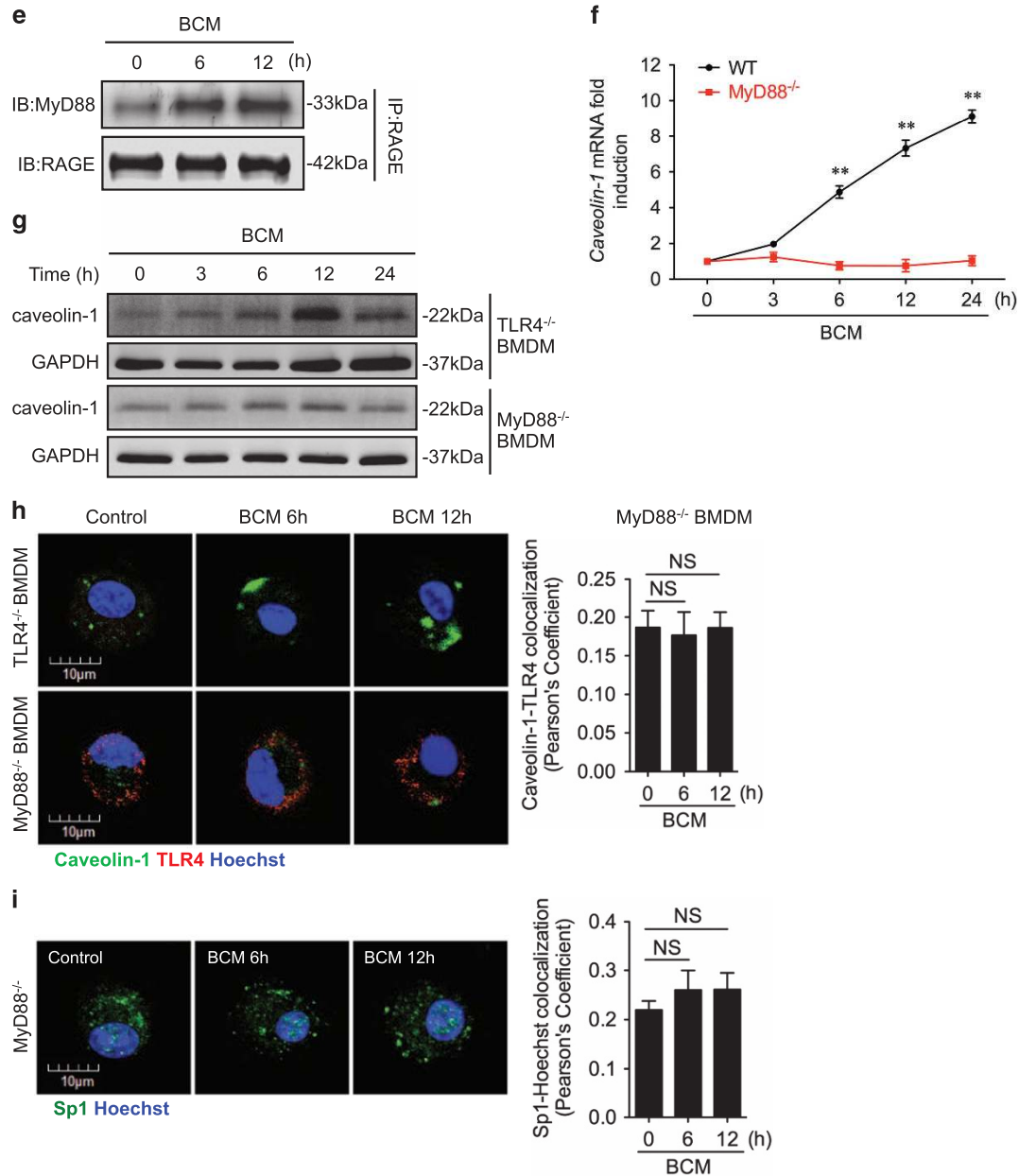


Figure 5 Continued

within the BCM acts through RAGE signaling and is a major component mediating tissue damage-suppressed M $\phi$  necroptosis in response to LPS.

Necroptosis is a regulated form of inflammatory cell death. Previous studies showed that necroptosis can be triggered by members of the pattern recognition receptor family, which including Toll-like receptors, NOD-like receptors, and retinoic acid-inducible gene I-like receptors.<sup>5,52-54</sup> LPS-induced cell necroptosis contributes to inflammation cascade.<sup>3</sup> In this study, we defined that macrophage necroptosis is a major form of cell death in response to LPS. We showed that necroptosis inhibitor Nec-1 s effectively prevented LPS-induced macrophage death; whereas, ferroptosis inhibitor Fer-1 and pan-caspase

inhibitor z-VAD-FMK, which suppresses apoptosis and pyroptosis, failed to reduce LPS-induced macrophage death. We further showed that M $\phi$  surface expression of TLR4 is a determinant for LPS-induced necroptosis, and TLR4 internalization, and subsequent desensitization of cells to LPS, results in attenuation of M $\phi$  necroptosis. Our *in vivo* and *in vitro* studies also show that associated with decreased M $\phi$  necroptosis, M $\phi$ -originated inflammation, including cytokines IL-6 and TNF $\alpha$  expression and secretion, is ameliorated as well (Figure 6), suggesting that reduced TLR4 surface levels secondary to remote tissue damage desensitize macrophage cytokine responses to LPS. Of note, the negative regulating effect of tissue damage also has a temporal component,

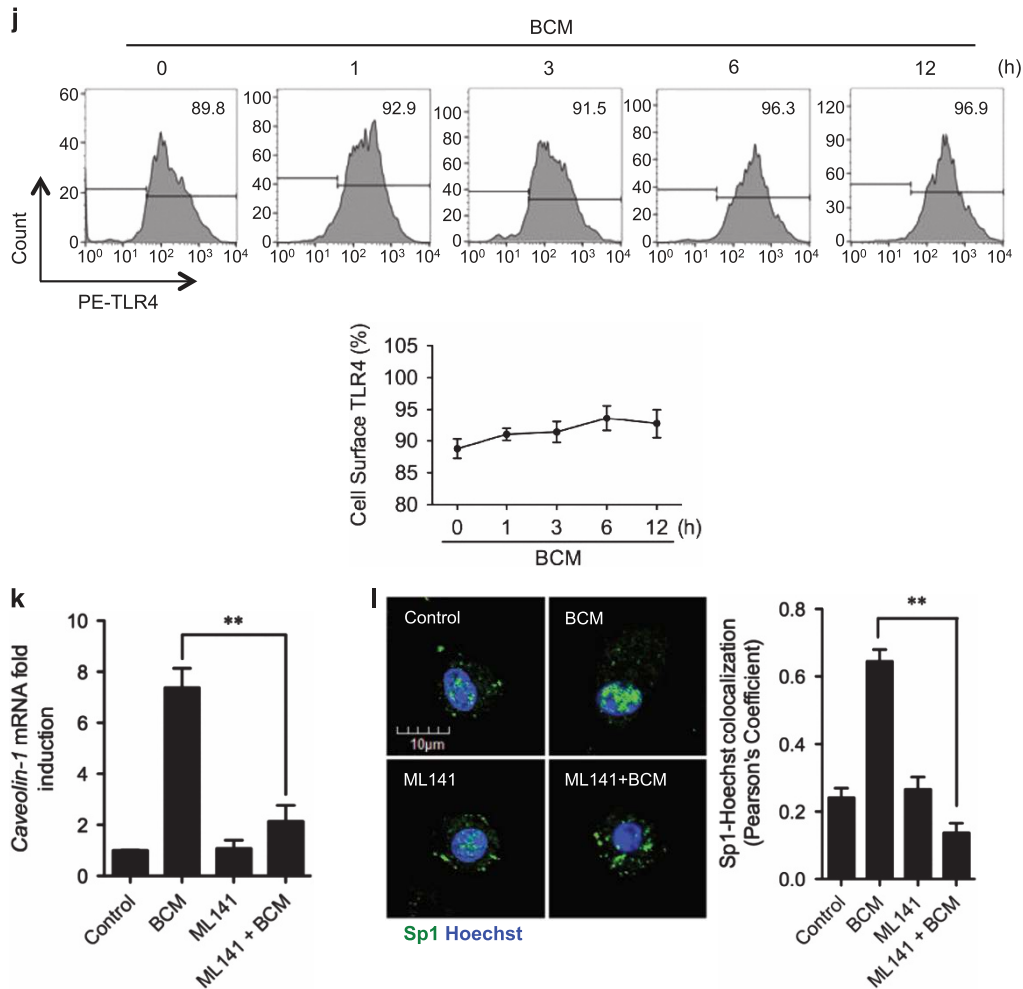


Figure 5 Continued

appearing at 12–48 h after injury when HMGB1/RAGE signaling leads to TLR4 internalization. At later time points recovery of cell surface expression of TLR4 might theoretically weaken this tissue damage-mediated effect on inflammatory responses to LPS/infection. Importantly, our data suggest that the DAMPs not only facilitate inflammation in disease processes without overt infection,<sup>55</sup> but can also negatively regulate Mφ responses to pathogen-associated molecular patterns (PAMPs), such as LPS.

In the context of tissue injury and inflammation, RAGE and TLRs have critical roles in recognizing and interacting with DAMP and PAMP molecules.<sup>56,57</sup> Receptor cross-talk between RAGE and TLR4 has not been studied previously. In the current study, we demonstrated that tissue-damage release of DAMPs act through RAGE signaling and caveolin-1-dependent pathway to induce Mφ surface TLR4 internalization, suggesting that RAGE and TLR4 may reciprocally regulate the function of the other in response to both trauma and infection.

In summary, our study demonstrates a novel role for tissue damage release of DAMP molecule HMGB1 to suppress LPS-induced Mφ necroptosis and inflammation.

This finding suggests a previously unidentified protective role of DAMPs in restricting inflammation in response to exogenous PAMPs.

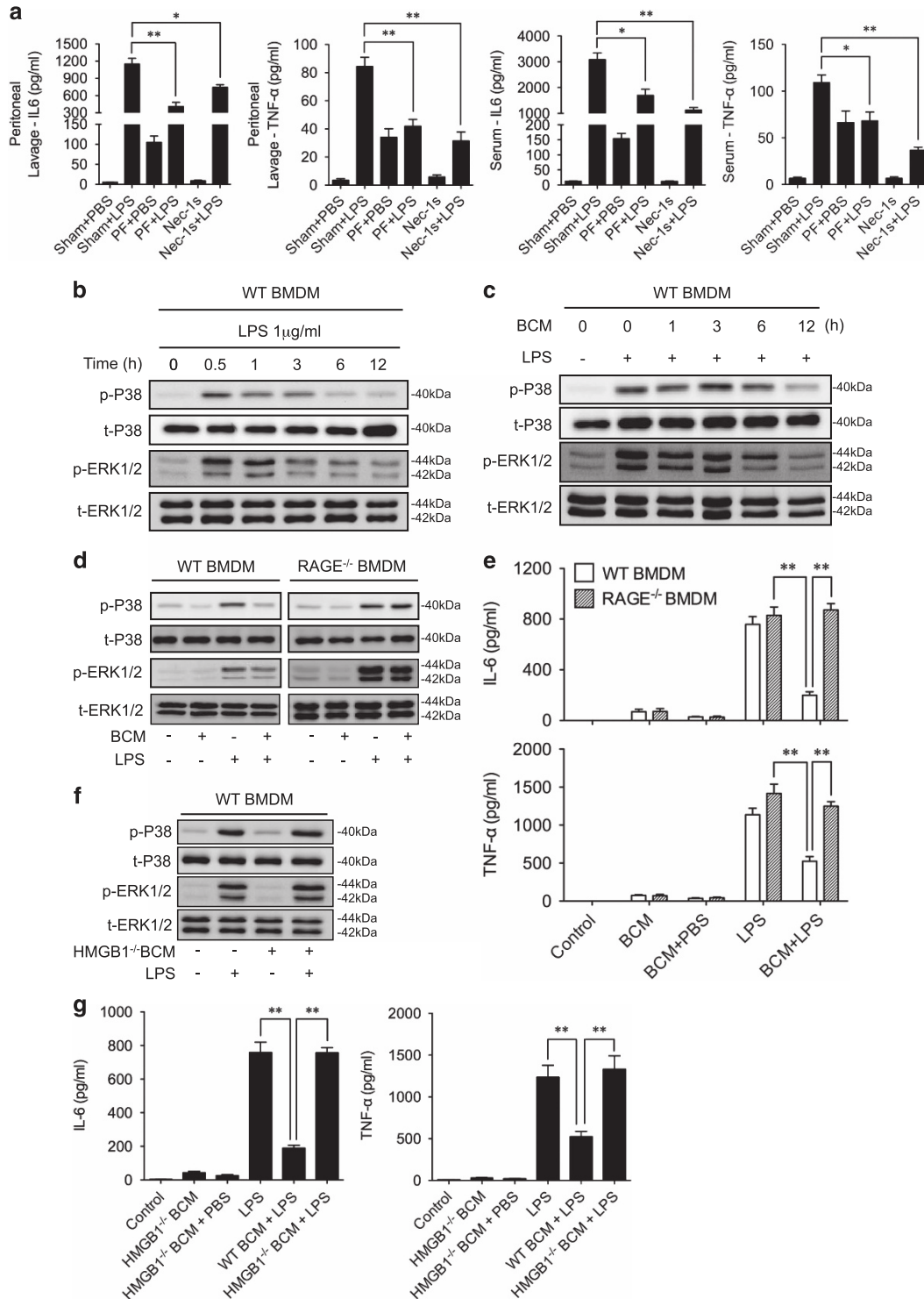
#### Materials and Methods

**Animal strains.** C57BL/6 WT mice were purchased from The Jackson Laboratory (Bar Harbor, ME, USA). RAGE knockout ( $RAGE^{-/-}$ ) mice, TLR4 knockout ( $TLR4^{-/-}$ ) mice, myeloid differentiation primary response gene 88 knockout ( $MyD88^{-/-}$ ) mice, and inducible HMGB1-knockout (HMGB1-deficient) mice, all on a C57BL/6 background, were obtained from Dr. Billiar's laboratory at the University of Pittsburgh. All animal experimental protocols were reviewed and approved by the Institutional Animal Care and Use Committees of University of Pittsburgh and VA Pittsburgh Healthcare System.

**Mouse PF model.** Femurs and tibias from a euthanized donor mouse were crushed using a sterile mortar and 0.5 g of the bone crush was homogenized in 2 ml sterile PBS to become the BCM. The recipient mouse was anesthetized with ketamine (50 mg/kg BW) and xylazine (5 mg/kg BW) and the thighs were squeezed with a hemostat for 30 s to induce a soft-tissue lesion, followed by injection of 0.15 ml of the BCM in the tissue lesion area.<sup>24</sup> Sham animals underwent the same anesthesia procedure and injection of 0.15 ml of normal saline at the thighs. In some animals, at 12 h after the injection of BCM or saline, were intraperitoneally administered LPS (2 mg/kg BW in 0.2 ml of PBS).

**BMDM isolation and culture.** Bone marrow was flushed out with pre-chilled Dulbecco's Modified Eagle Medium (DMEM) from femurs and tibias, which were harvested from WT and the above-mentioned gene knockout mice following the previously described method.<sup>58,59</sup> In brief, cell pellets were collected by centrifugation at 4 °C, and erythrocytes were lysed with RBC lysis buffer

(eBioscience, San Diego, CA, USA). The resultant cells were then washed two times with PBS and suspended in BMDM culture medium (DMEM containing 10% fetal bovine serum complemented with 50 μg/ml penicillin/streptomycin and 10 ng/ml recombinant macrophage-colony stimulating factor (M-CSF; Sigma-Aldrich, St Louis, MO, USA)) at a concentration of 10<sup>6</sup> cells/ml and seeded into 6-cm ultra-low





attachment surface plates (Corning Costar, Corning, NY, USA). The BMDM culture medium was changed on day 3 and day 5. BMDM were fully differentiated and ready for use at day 7.

**Cell staining.** BMDM were seeded in the glass bottom petri dish (P35G-0-10-C, MatTek Corporation, Ashland, MA, USA) and fixed with 4% paraformaldehyde for 15 min at room temperature. After washing with PBS, the cells were permeabilized with 0.01% Triton X-100 in PBS for 15 min at room temperature, followed by blocking with 5% bovine serum albumin in PBS for 1 h at room temperature. The cells were then incubated with a primary antibody at 4 °C overnight, followed by incubation with fluorescence-conjugated secondary antibody for 1 h at room temperature. Cell nucleus was stained with Hoechst 33258 (Sigma-Aldrich). The BMDM were then measured by confocal microscopy (Olympus, Fluoview-FV1000, Olympus America Co., Center Valley, PA, USA).

**Western blot.** BMDM lysates were separated by 8 and 12% SDS-PAGE, and then were transferred onto PVDF membranes. After blocking for 1 h at room temperature with blocking buffer (LI-COR Biosciences, Lincoln, NE, USA), blots were incubated with the primary antibody at 4 °C overnight, followed by incubation

with the appropriate secondary antibodies (LI-COR Biosciences) for 1 h. Protein bands were detected using the Odyssey System from LI-COR Biosciences.

**RNA extraction and quantitative real-time PCR.** Total RNA was isolated from BMDM using TRIzol RNA Isolation Reagents (Life Technologies, Pittsburgh, PA, USA) by following the instructions. Real-time RT-PCR was done using the SsoAdvanced Universal SYBR Green Supermix (172-5271, Bio-Rad, Hercules, CA, USA) in a Bio-Rad iQ5 real-time PCR machine (Bio-Rad). The following gene-specific primers were used for amplifying genes: *Caveolin-1* forward, 5'-GCAGAACCAGAAGGGAC-3', and reverse, 5'-TAGACAACAAGCGGTAAAA-3'; and *GAPDH* forward, 5'-AACCTGCCAAGTATGATGA-3' and reverse, 5'-GGAGTTGCTGTGAAGTC-3'. Reverse transcription was done using iScript Reverse Transcription Supermix (170-8840, Bio-Rad) following the manufacturer's instructions. Amplification was performed with cycling conditions of 95 °C for 15 s then 60 °C for 30 s for 40 cycles. After amplification protocol was over, PCR product was subjected to melt-curve analysis using Bio-Rad iQ5 software (Bio-Rad). Fold change was calculated using the  $\Delta\Delta$  threshold cycle method<sup>60</sup> and the value for the *GAPDH* gene, which was normalized to untreated groups.

**Reagents.** Primary antibodies for cell staining were: RIPK1 antibody (610458, BD Biosciences, San Jose, CA, USA), RIPK3 antibody (sc-135170, Santa Cruz Biotechnology, Dallas, TX, USA), TLR4 antibody (sc-30002, Santa Cruz Biotechnology), Alexa Fluor 488-conjugated-Caveolin-1 antibody (NB100-615AF488, Novus Biologicals, Littleton, CO, USA), and Sp1 antibody (sc-59, Santa Cruz Biotechnology). Secondary antibodies including Alexa Fluor 488-conjugated anti-mouse IgG, Cy3-conjugated anti-rabbit IgG, and Alexa Fluor 488-conjugated anti-rabbit IgG were provided by the Center for Biologic Imaging, University of Pittsburgh Medicine Center.

Primary antibodies used for western blotting include TLR4 antibody (sc-30002, Santa Cruz Biotechnology), anti-RIPK1 antibody (610458, BD Biosciences), anti-RIPK3 (2283, ProSci, Fort Collins, CO, USA), anti-MLKL phosphor S345 (ab196436, abcam, Cambridge, MA, USA), Caveolin-1 antibody (sc-894, Santa Cruz Biotechnology), Phospho-p38 MAPK (Thr180/Tyr182) (3D7) XP Rabbit mAb (#9215, Cell Signaling Technology, Danvers, MA, USA), p38 MAPK(D13E1) XP Rabbit mAb (#8690, Cell Signaling Technology), Phospho-p44/42 MAPK (ERK1/2) (Thr202/Tyr204) (D12.14.4E) XP Rabbit mAb (#4370, Cell Signaling Technology), p44/42 MAPK (Erk1/2) (137F5) Rabbit mAb (#4695, Cell Signaling Technology), GAPDH (D16H11) XP Rabbit mAb (#5174 Cell Signaling Technology), MyD88 antibody (sc-8197, Santa Cruz Biotechnology), RAGE (ab37647, abcam), and HMGB1 antibody (ab18256, abcam).

Annexin V detection Kit was from BD Biosciences. Anti-Mouse CD284 (TLR4) PE (12-9041-80) for detecting cell surface TLR4, anti-Mouse F4/80 Antigen FITC (11-4801-81), anti-Mouse CD43 PE (12-0431-81), anti-Mouse Ly6C PE-Cyanine7 (25-5932-80), mouse IL-6 ELISA kit (88-7064-86), and mouse TNF alpha ELISA kit (88-7324-86) were purchased from eBioscience. Dynabeads Protein G Immunoprecipitation Kit (10007D) and Pierce Co-Immunoprecipitation Kit (26149) for immunoprecipitation was from Thermo Fisher Scientific (Pittsburgh, PA, USA). Necroptosis inhibitor Nec-1 s (2263-1) was purchased from BioVision (Milpitas, CA, USA). Pan-caspase inhibitor z-VAD-FMK (V116-2MG) and ferroptosis inhibitor Fer-1 (SML0583-5MG) was from Sigma-Aldrich. Sp1 inhibitor Mithramycin A (11434) was obtained from Cayman Chemical (Ann Arbor, MI, USA). Cdc42 inhibitor ML141 (sc-362768) was from Santa Cruz Biotechnology. Recombinant HMGB1 (1690-HMB-050) was from R&D Systems (Minneapolis, MN, USA).

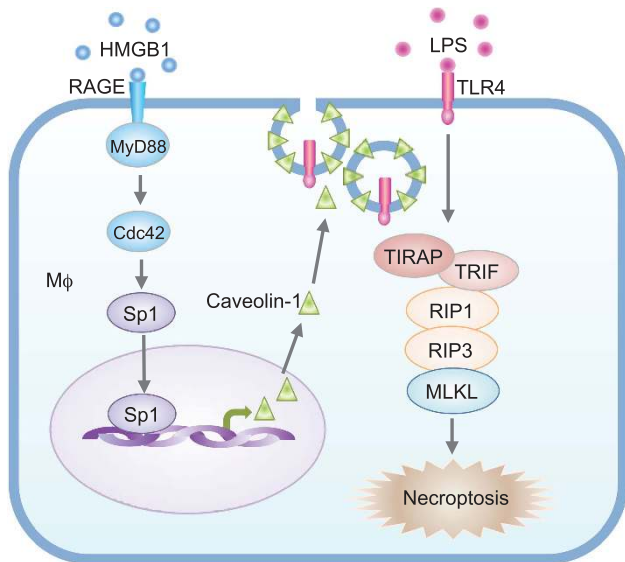


**Figure 7** Model of the mechanism underlying tissue-damage regulation of LPS-induced Mφ necroptosis. LPS acting through TLR4 promotes Mφ necroptosis. However, damaged tissue through HMGB1/RAGE signaling upregulates caveolin-1 expression in Mφ, which, in turn, induces caveolae-mediated TLR4 internalization and desensitization, thereby, ameliorates LPS-TLR4-induced Mφ necroptosis. RAGE-MyD88 signal activation of Cdc42 and the consequent nuclear translocation of Sp1 serve the mechanism of upregulation of caveolin-1

**Figure 6** Tissue damage suppresses LPS-induced inflammation. (a) WT mice were subjected to one of the following six groups: (1) Sham for 12 h followed by PBS (vehicle, 0.2 ml i.p.) (Sham+PBS); (2) Sham for 12 h followed by LPS (2 mg/kg BW in 0.2 ml of PBS i.p.) for 6 h (Sham+LPS); (3) Pseudo-fracture (PF) for 12 h followed by PBS (0.2 ml i.p.) (PF+PBS); (4) PF for 12 h followed by LPS (2 mg/kg BW i.p. in 0.2 ml of PBS for 6 h) (PF+LPS); (5) Nec-1 s (30 mmol/kg BW i.p. in 0.2 ml of PBS) for 6 h (Nec-1 s); and (6) Nec-1 s (30 mmol/kg BW i.p.) and LPS (2 mg/kg BW i.p. in 0.2 ml of PBS) for 6 h (Nec-1 s+LPS). The peritoneal lavage fluid and serum were then collected for measurement of IL-6 and TNF- $\alpha$  by ELISA. (b) WT BMDM were treated with LPS (1  $\mu$ g/ml) for 0–12 h, and the phosphorylation of P38 and ERK1/2 MAPK were then detected by western blot. (c) WT BMDM were pretreated with BCM (40  $\mu$ l/ml) for 0–12 h, and then were washed for three times followed by treatment with LPS (1  $\mu$ g/ml) 0.5 h. Phosphorylation of P38 and ERK1/2 MAPK were detected by western blot. (d) WT or RAGE<sup>-/-</sup> BMDM were pretreated with BCM (40  $\mu$ l/ml) for 12 h, and then were washed for three times followed by the treatment with LPS (1  $\mu$ g/ml) for 0.5 h. Phosphorylation of P38 and ERK1/2 MAPK were detected by western blot. (e) WT and RAGE<sup>-/-</sup> BMDM were pretreated with BCM (40  $\mu$ l/ml) for 12 h, and then were washed for three times followed by the treatment with LPS (1  $\mu$ g/ml) for 6 h. IL-6 and TNF- $\alpha$  concentration in the supernatant were then measured by ELISA. (f) WT BMDM were pretreated with WT or HMGB1-lacking BCM (40  $\mu$ l/ml) for 12 h, and then were washed for three times followed by the treatment with LPS (1  $\mu$ g/ml) for 0.5 h. Phosphorylation of P38 and ERK1/2 MAPK were then detected western blot. (g) WT BMDM were pretreated with WT or HMGB1-lacking BCM (40  $\mu$ l/ml) for 12 h, and then were washed for three times followed by the treatment with LPS (1  $\mu$ g/ml) for 6 h. IL-6 and TNF- $\alpha$  in the supernatant were measured by ELISA. All results are representative of three independent experiments. The graphs show the mean and S.E.M., n = 3. \*P < 0.05 and \*\*P < 0.01 compares between the indicated groups



**Data presentation and statistical analysis.** The data are presented as mean  $\pm$  S.E.M. of the indicated number of experiments. SPSS 19.0 was used for statistical analysis. Significances between groups were determined by using one-way ANOVA or two-tailed Student's *t*-test.  $P < 0.05$  was considered as statistically significant.

### Conflict of Interest

The authors declare no conflict of interest.

**Acknowledgements.** This work was supported by the National Institutes of Health Grant R01-HL-079669 (JF and MAW), National Institutes of Health Center Grant P50-GM-53789 (TRB and JF), National Institutes of Health Grant R56-HL-123882 (JF), VA Merit Award 1I01BX002729 (JF), National Key Basic Research Program 2010CB529704 (JY China), PCSIRT IRT0731 (JY), and National Natural Science Foundation of China 30670828 (JY).

### Author contributions

ZL, YL, EF, JL planned and did experiments including cell isolation and treatment, confocal microscopy, western blotting, and flow cytometry; ZL, YL did animal experiments; GX, SL, TRB, MAW, YJ, and JF planned the project and conceived the experiments; ZL, YJ, EF, MJS, and JF conceived the data and wrote the manuscript.

- Cooper RA. Surgical site infections: epidemiology and microbiological aspects in trauma and orthopaedic surgery. *Int Wound J* 2013; **10**(Suppl 1): 3–8.
- Xu J, Jiang Y, Wang J, Shi X, Liu Q, Liu Z *et al*. Macrophage endocytosis of high-mobility group box 1 triggers pyroptosis. *Cell Death Differ* 2014; **21**: 1229–1239.
- Feoktistova M, Leverkus M. Programmed necrosis and necroptosis signalling. *FEBS J* 2015; **282**: 19–31.
- Kaczmarek A, Vandenabeele P, Krysko DV. Necroptosis: the release of damage-associated molecular patterns and its physiological relevance. *Immunity* 2013; **38**: 209–223.
- Vanden Berghe T, Linkermann A, Jouan-Lanhouet S, Walczak H, Vandenabeele P. Regulated necrosis: the expanding network of non-apoptotic cell death pathways. *Nat Rev Mol Cell Biol* 2014; **15**: 135–147.
- Wang H, Bloom O, Zhang M, Vishnubhakat JM, Ombrellino M, Che J *et al*. HMGB-1 as a late mediator of endotoxin lethality in mice. *Science* 1999; **285**: 248–251.
- Martino F, Petrilli V, Mayor A, Tardivel A, Tschopp J. Gout-associated uric acid crystals activate the NALP3 inflammasome. *Nature* 2006; **440**: 237–241.
- Lu B, Nakamura T, Inouye K, Li J, Tang Y, Lundback P *et al*. Novel role of PKR in inflammasome activation and HMGB1 release. *Nature* 2012; **488**: 670–674.
- Andersson U, Tracey KJ. HMGB1 is a therapeutic target for sterile inflammation and infection. *Annu Rev Immunol* 2011; **29**: 139–162.
- Bucciarelli LG, Wendt T, Rong L, Lalla E, Hofmann MA, Goova MT *et al*. RAGE is a multiligand receptor of the immunoglobulin superfamily: implications for homeostasis and chronic disease. *Cell Mol Life Sci* 2002; **59**: 1117–1128.
- van Zoelen MA, Schmidt AM, Florquin S, Meijers JC, de Beer R, de Vos AF *et al*. Receptor for advanced glycation end products facilitates host defense during Escherichia coli-induced abdominal sepsis in mice. *J Infect Dis* 2009; **200**: 765–773.
- Huttunen HJ, Kuja-Panula J, Sorci G, Agneletti AL, Donato R, Rauvala H. Coregulation of neurite outgrowth and cell survival by amphotericin and S100 proteins through receptor for advanced glycation end products (RAGE) activation. *J Biol Chem* 2000; **275**: 40096–40105.
- Toure F, Zahm JM, Garnotel R, Lambert E, Bonnet N, Schmidt AM *et al*. Receptor for advanced glycation end-products (RAGE) modulates neutrophil adhesion and migration on glycoxidated extracellular matrix. *Biochem J* 2008; **416**: 255–261.
- Palumbo R, De Marchis F, Pusterla T, Conti A, Alessio M, Bianchi ME. Src family kinases are necessary for cell migration induced by extracellular HMGB1. *J Leukoc Biol* 2009; **86**: 617–623.
- Kim JY, Park HK, Yoon JS, Kim SJ, Kim ES, Ahn KS *et al*. Advanced glycation end product (AGE)-induced proliferation of HEL cells via receptor for AGE-related signal pathways. *Int J Oncol* 2008; **33**: 493–501.
- Hudson BI, Kalea AZ, Del Mar Arriero M, Harja E, Boulanger E, D'Agati V *et al*. Interaction of the RAGE cytoplasmic domain with diaphanous-1 is required for ligand-stimulated cellular migration through activation of Rac1 and Cdc42. *J Biol Chem* 2008; **283**: 34457–34468.
- Sorci G, Riuzzi F, Giambanco I, Donato R. RAGE in tissue homeostasis, repair and regeneration. *Biochim Biophys Acta* 2013; **1833**: 101–109.
- Rajaiah R, Perkins DJ, Ireland DD, Vogel SN. CD14 dependence of TLR4 endocytosis and TRIF signaling displays ligand specificity and is dissociable in endotoxin tolerance. *Proc Natl Acad Sci USA* 2015; **112**: 8391–8396.
- Roy S, Karmakar M, Pearlman E. CD14 mediates Toll-like receptor 4 (TLR4) endocytosis and spleen tyrosine kinase (Syk) and interferon regulatory transcription factor 3 (IRF3) activation in epithelial cells and impairs neutrophil infiltration and *Pseudomonas aeruginosa* killing in vivo. *J Biol Chem* 2014; **289**: 1174–1182.

- Husebye H, Halaas O, Stenmark H, Tunheim G, Sandanger O, Bogen B *et al*. Endocytic pathways regulate Toll-like receptor 4 signaling and link innate and adaptive immunity. *EMBO J* 2006; **25**: 683–692.
- Parton RG, Simons K. The multiple faces of caveolae. *Nat Rev Mol Cell Biol* 2007; **8**: 185–194.
- He K, Yan X, Li N, Dang S, Xu L, Zhao B *et al*. Internalization of the TGF-beta type I receptor into caveolin-1 and EEA1 double-positive early endosomes. *Cell Res* 2015; **25**: 738–752.
- Kobbe P, Vodovotz Y, Kaczorowski DJ, Billiar TR, Pape HC. The role of fracture-associated soft tissue injury in the induction of systemic inflammation and remote organ dysfunction after bilateral femur fracture. *J Orthop Trauma* 2008; **22**: 385–390.
- Darwiche SS, Kobbe P, Pfeifer R, Kohut L, Pape HC, Billiar T. Pseudofracture: an acute peripheral tissue trauma model. *J Vis Exp* 2011: 50.
- Kohut LK, Darwiche SS, Brumfield JM, Frank AM, Billiar TR. Fixed volume or fixed pressure: a murine model of hemorrhagic shock. *J Vis Exp* 2011: 52.
- Wu XN, Yang ZH, Wang XK, Zhang Y, Wan H, Song Y *et al*. Distinct roles of RIP1-RIP3 hetero- and RIP3-RIP3 homo-interaction in mediating necroptosis. *Cell Death Differ* 2014; **21**: 1709–1720.
- Li J, McQuade T, Siemer AB, Napetschnig J, Moriwaki K, Hsiao YS *et al*. The RIP1/RIP3 necrosome forms a functional amyloid signaling complex required for programmed necrosis. *Cell* 2012; **150**: 339–350.
- Smith CC, Necroptosis Yellon DM. Necrostatins and tissue injury. *J Cell Mol Med* 2011; **15**: 1797–1806.
- Ekert PG, Silke J, Vaux DL. Caspase inhibitors. *Cell Death Differ* 1999; **6**: 1081–1086.
- McComb S, Cheung HH, Korneluk RG, Wang S, Krishnan L. cIAP1 and cIAP2 limit macrophage necroptosis by inhibiting Rip1 and Rip3 activation. *Cell Death Differ* 2012; **19**: 1791–1801.
- Thapa RJ, Nogusa S, Chen P, Maki JL, Lerro A, Andrade M *et al*. Interferon-induced RIP1/RIP3-mediated necrosis requires PKR and is licensed by FADD and caspases. *Proc Natl Acad Sci USA* 2013; **110**: E3109–E3118.
- Poltorak A, He X, Smirnova I, Liu MY, Van Huffel C, Du X *et al*. Defective LPS signaling in C3H/HeJ and C57BL/10ScCr mice: mutations in Tlr4 gene. *Science* 1998; **282**: 2085–2088.
- Miller SI, Ernst RK, LPS Bader MW. TLR4 and infectious disease diversity. *Nat Rev Microbiol* 2005; **3**: 36–46.
- Peltz ED, Moore EE, Eckels PC, Damle SS, Tsuruta Y, Johnson JL *et al*. HMGB1 is markedly elevated within 6 hours of mechanical trauma in humans. *Shock* 2009; **32**: 17–22.
- Xiang M, Yuan Y, Fan L, Li Y, Li A, Yin L *et al*. Role of macrophages in mobilization of hematopoietic progenitor cells from bone marrow after hemorrhagic shock. *Shock* 2012; **37**: 518–523.
- Kang R, Zhang Q, Hou W, Yan Z, Chen R, Bonaroti J *et al*. Intracellular Hmgb1 inhibits inflammatory nucleosome release and limits acute pancreatitis in mice. *Gastroenterology* 2014; **146**: 1097–1107.
- Kokkola R, Andersson A, Mullins G, Ostberg T, Treutiger CJ, Arnold B *et al*. RAGE is the major receptor for the proinflammatory activity of HMGB1 in rodent macrophages. *Scand J Immunol* 2005; **61**: 1–9.
- Wang XM, Kim HP, Nakahira K, Ryter SW, Choi AM. The heme oxygenase-1/carbon monoxide pathway suppresses TLR4 signaling by regulating the interaction of TLR4 with caveolin-1. *J Immunol* 2009; **182**: 3809–3818.
- Dasari A, Bartholomew JN, Volonte D, Galbiati F. Oxidative stress induces premature senescence by stimulating caveolin-1 gene transcription through p38 mitogen-activated protein kinase/Sp1-mediated activation of two GC-rich promoter elements. *Cancer Res* 2006; **66**: 10805–10814.
- Sleiman SF, Langley BC, Basso M, Berlin J, Xia L, Payappilly JB *et al*. Mithramycin is a gene-selective Sp1 inhibitor that identifies a biological intersection between cancer and neurodegeneration. *J Neurosci* 2011; **31**: 6858–6870.
- Blume SW, Snyder RC, Ray R, Thomas S, Koller CA, Miller DM. Mithramycin inhibits SP1 binding and selectively inhibits transcriptional activity of the dihydrofolate reductase gene in vitro and in vivo. *J Clin Invest* 1991; **88**: 1613–1621.
- Surviladze Z, Waller A, Strouse JJ, Bologna C, Ursu O, Salas V *et al*. A Potent and Selective Inhibitor of Cdc42 GTPase. *Probe Reports from the NIH Molecular Libraries Program*. National Center for Biotechnology Information (US); Bethesda (MD), 2010, pp 1–27.
- Tamemoto H, Kadowaki T, Tobe K, Ueki K, Izumi T, Chatani Y *et al*. Biphasic activation of two mitogen-activated protein kinases during the cell cycle in mammalian cells. *J Biol Chem* 1992; **267**: 20293–20297.
- Meja KK, Seldon PM, Nasuhara Y, Ito K, Barnes PJ, Lindsay MA *et al*. p38 MAP kinase and MKK-1 co-operate in the generation of GM-CSF from LPS-stimulated human monocytes by an NF-kappa B-independent mechanism. *Br J Pharmacol* 2000; **131**: 1143–1153.
- Fan J, Li Y, Vodovotz Y, Billiar TR, Wilson MA. Hemorrhagic shock-activated neutrophils augment TLR4 signaling-induced TLR2 upregulation in alveolar macrophages: role in hemorrhage-primed lung inflammation. *Am J Physiol Lung Cell Mol Physiol* 2006; **290**: L738–L746.
- Fan J, Li Y, Levy RM, Fan JJ, Hackam DJ, Vodovotz Y *et al*. Hemorrhagic shock induces NAD(P)H oxidase activation in neutrophils: role of HMGB1-TLR4 signaling. *J Immunol* 2007; **178**: 6573–6580.
- Xiang M, Yin L, Li Y, Xiao G, Vodovotz Y, Billiar TR *et al*. Hemorrhagic shock activates lung endothelial reduced nicotinamide adenine dinucleotide phosphate (NADPH) oxidase via neutrophil NADPH oxidase. *Am J Respir Cell Mol Biol* 2011; **44**: 333–340.

48. Xiang M, Shi X, Li Y, Xu J, Yin L, Xiao G *et al*. Hemorrhagic shock activation of NLRP3 inflammasome in lung endothelial cells. *J Immunol* 2011; **187**: 4809–4817.
49. Xu P, Wen Z, Shi X, Li Y, Fan L, Xiang M *et al*. Hemorrhagic shock augments Nlrp3 inflammasome activation in the lung through impaired pyrin induction. *J Immunol* 2013; **190**: 5247–5255.
50. Wen Z, Fan L, Li Y, Zou Z, Scott MJ, Xiao G *et al*. Neutrophils counteract autophagy-mediated anti-inflammatory mechanisms in alveolar macrophage: role in posthemorrhagic shock acute lung inflammation. *J Immunol* 2014; **193**: 4623–4633.
51. Jiao H, Zhang Y, Yan Z, Wang ZG, Liu G, Minshall RD *et al*. Caveolin-1 Tyr14 phosphorylation induces interaction with TLR4 in endothelial cells and mediates MyD88-dependent signaling and sepsis-induced lung inflammation. *J Immunol* 2013; **191**: 6191–6199.
52. Pasparakis M, Vandenabeele P. Necroptosis and its role in inflammation. *Nature* 2015; **517**: 311–320.
53. He S, Liang Y, Shao F, Wang X. Toll-like receptors activate programmed necrosis in macrophages through a receptor-interacting kinase-3-mediated pathway. *Proc Natl Acad Sci USA* 2011; **108**: 20054–20059.
54. Humphries F, Yang S, Wang B, Moynagh PN. RIP kinases: key decision makers in cell death and innate immunity. *Cell Death Differ* 2015; **22**: 225–236.
55. Yang H, Antoine DJ, Andersson U, Tracey KJ. The many faces of HMGB1: molecular structure-functional activity in inflammation, apoptosis, and chemotaxis. *J Leukoc Biol* 2013; **93**: 865–873.
56. Beutler B. Tlr4: central component of the sole mammalian LPS sensor. *Curr Opin Immunol* 2000; **12**: 20–26.
57. Ibrahim ZA, Armour CL, Phipps S, Sukkar MB. RAGE and TLRs: relatives, friends or neighbours? *Mol Immunol* 2013; **56**: 739–744.
58. Weischenfeldt J, Porse B. Bone marrow-derived macrophages (BMM): isolation and applications. *CSH Protoc* 2008 pdb prot5080.
59. Francke A, Herold J, Weinert S, Strasser RH, Braun-Dullaeus RC. Generation of mature murine monocytes from heterogeneous bone marrow and description of their properties. *J Histochem Cytochem* 2011; **59**: 813–825.
60. Livak KJ, Schmittgen TD. Analysis of relative gene expression data using real-time quantitative PCR and the 2(-Delta Delta C(T)) Method. *Methods* 2001; **25**: 402–408.